Title:

CREB-binding protein gene, *HAC701*, negatively regulates WRKY45-dependent immunity in rice

Running title:

HAC701-dependent immunity regulation

Authors:

Nino A. Espinas[1,4,*], Tu Ngoc Le[1,2], Saori, Miura[1], Yasuka Shimajiri[1,3], Ken Shirasu[4], Hidetoshi Saze[1]

Affiliation:

[1]Okinawa Institute of Science and Technology Graduate University, Onna-son, Okinawa, Japan

[2]Bioinformation and DDBJ Center, National Institute of Genetics, Mishima, Shizuoka, Japan

[3]EditForce, Fukuoka, Japan

[4]RIKEN Center for Sustainable Resource Science, Yokohama, Kanagawa, Japan

Contact:

[*]Correspondence to: Nino A. Espinas (nino.espinas@riken.jp)

Category:

Biological Sciences, Plant Biology

SIGNIFICANCE

HAC701 is a member of CREB-binding protein (CBP) family that acts as transcriptional coactivator and acetyltransferase. However, little is known how it regulates innate immunity in plants. Herein we reported that rice *HAC701* suppresses WRKY45-dependent defense pathway. Our study showed that *HAC701* seemingly interacts genetically with *WRKY45* in rice to modulate immune responses against pathogens.

ABSTRACT

CREB-binding protein (CBP) is a known transcriptional coactivator and an acetyltransferase that functions in several cellular processes by regulating gene expression. However, how it functions in plant immunity remains unexplored. By characterizing *hac701*, we demonstrate that *HAC701* negatively regulates the immune responses in rice. *hac701* shows enhanced disease resistance against a bacterial pathogen, *Pseudomonas syringae* pv. *oryzae* (*Pso*), which causes bacterial halo blight of rice. Our transcriptomic analysis revealed that rice *WRKY45*, one of the main regulators of rice immunity, is upregulated in *hac701* and possibly conferring the resistance phenotype against *Pso*. The morphological phenotypes of *hac701* single mutants were highly similar to *WRKY45* overexpression transgenic lines reported in previous studies. In addition, we also compared the list of genes in these studies when *WRKY45* is overexpressed and chemically induced transiently with the differentially expressed genes (DEGs) in *hac701*, and found that they largely overlap. When we investigated for *cis*-elements found 1kb upstream of *WRKY45* gene and WRKY45-dependent DEGs, we found that *WRKY45* promoter contains the CRE motif, a possible target of HAC701-mediated regulation. Genome-wide H3K9 acetylation profiling showed depletion of acetylation at large set of genes in *hac701*. However, consistent with the upregulation of *WRKY45* gene expression, our ChIP-sequencing analysis demonstrated that regions of *WRKY45* promoter are enriched in H3K9 acetylation in *hac701* compared to the segregated wild type control in the mock condition. *WRKY45* promoter might be on the receiving end for possible genome-wide compensatory effects when a global regulator like *HAC701* is mutated. Finally, we show that *HAC701* may have roles in systemic immune signaling. We therefore propose that wild type *HAC701* negatively regulates *WRKY45* gene expression, thereby suppressing immune responses.

Keywords:

Oryza sativa, rice CREB-binding protein, *HAC701*, *WRKY45*, innate immunity, *Pseudomonas syringae* pv. *oryzae* (*Pso*), *Magnaporthe*

INTRODUCTION

Histone acetyltransferases (HATs) are a diverse group of histone- and non-histone-modifying enzymes that contain multiple subunits to enable catalytic functions (1). These HATs primarily function as scaffolding bridges of proteins to form the transcriptional regulatory complex important for target recognition and subsequent substrate modification (1-3). The association of HATs to its interacting proteins and the existing state of the epigenome dictates the dual-switch functionality of either transcriptional activation or repression (1). They are considered integrators or adaptors as they were shown to interact with DNA-binding activators and the basal transcriptional machinery (4, 5).

In plant model Arabidopsis, HATs and histone deacetylases (HDACs) are grouped into four (Figure 1A) and three families, respectively (6). HATs consists of CBP, TAF1/TAFII250, GNAT, and MYST, while HDACs are RPD3/HDA1, HD2-like, and SIR2. A previous review of HATs and HDACs in plants listed about 12 putative HAT and 18 HDAC proteins exhibiting acetylation and deacetylation activities with differential site specificities (6). Work on rice (*Oryza sativa*), however, has just begun with a preliminary investigation of eight histone acetyltransferases (7, 8) and deacetylases (9).

Several studies have shown that histone acetylation and deacetylation control defense signaling in plants in response to phytohormone or pathogen application (10-12). More specifically, HATs and HDACs in rice model were shown to be responsive to abiotic stresses and can be modulated by phytohormones, thus implicating a role in biotic stresses (7, 13). Similar to Arabidopsis, HATs in rice are also classified into four families (Figure 1A) (7). In contrary, rice HDACs are represented in only two families, RPD3/HDA1-like and SIR2-like with no known rice member belonging to HD2 family (9).

110 *OsHAC701* was reported (14) earlier as a putative rice CBP-related acetyltransferase,
111 herein after referred to as *HAC701*, of the p300/CBP acetyltransferase (PCAT) family of
112 proteins. The Arabidopsis genome contains five CBP genes, while rice genome contains three
113 (Figure 1A), having broad acetyltransferase specificity on histones (7). Currently, there is no
114 clear consensus on the similarity of biological functions of Arabidopsis and rice homologs of
115 CBP family proteins. In animals, p300 and CBP are paralogs and originally described as
116 transcriptional coactivator that exhibit histone acetyltransferase activity on all four core
117 histones specifically at H4 N-terminal tail sites K5, K8, K12, and K16 (15, 16). Other sites
118 include H3 sites K14, 23 (17), K18, K27 (18, 19), and K56 (20); H2B sites are K12 and K15
119 (21). H3K9 is mainly acetylated by GCN5/PCAF (18), however acetylation by p300/CBP was
120 also reported (17, 22, 23). Its highly conserved function is mainly found in multicellular
121 organisms as it probably participates in complex physiological processes acting as a limiting
122 factor in various pathways due to its high cellular demand (14).

123 As HATs have been shown to be modulated by biotic stresses (24), we hypothesized
124 that it could be a potential system for studying rice immunity. Indeed, we show that *HAC701*
125 is involved in rice innate immunity. In this study, we have made CRISPR/Cas9 edited *hac701*
126 lines and showed that *HAC701* is apparently a negative regulator of immunity with the mutants
127 showing resistance against bacterial and fungal infection. Further transcriptomic investigation
128 showed that HAC701 possibly regulates *WRKY45* loci, one of the main regulators of rice
129 immunity pathways. In *hac701*, *WRKY45* and its direct and indirect gene targets were
130 upregulated upon pathogen inoculation. In addition, *hac701* phenocopies *WRKY45*-
131 overexpression (*WRKY45-ox*) lines, indicating a potential interaction between *HAC701* and
132 *WRKY45*-dependent immunity pathway in rice.

133

RESULTS

Characterization of a rice acetyltransferase mutant, *HAC701*.

We isolated null mutant lines by independently targeting two sites of *HAC701* gene (Fig. S1A-C; Fig. S1D-I) using CRISPR/Cas9 editing technology. From the 11 positive *HAC701* lines (Target 2), we have isolated four biallelic homozygous mutant lines (Fig. S1D), which we utilized for experimentation including their segregating wild type siblings, 9-WT (Fig. 1B). The phenotype in terms of effective grain number and tiller number of mostly all biallelic homozygous mutants at T2 generation did not show impairment as compared to 9-WT (Fig. S1F). In addition, the T3 lines did not show any visible growth or developmental defect in height and photosynthesis (*e.g.* chlorosis phenotype) (Fig. S1G), respectively. However, the weights of 1000-grain T3 and T4 generations of mutants were increased compared to 9-WT (Fig. S1I). These results indicate that a loss of HAC701 does not cause severe developmental defects in rice, and that HAC701 may have a positive role in seed production.

HAC701 mutant rice is resistant to pathogen infection.

Our expression analysis of the rice HAT genes showed that *HAC701* is significantly up-regulated by treatment of bacterial flg22 peptide, suggesting a potential role of HAC701 in plant defense against pathogens (Fig. S2). To investigate the involvement of *HAC701* in basal defense in rice, we inoculated 9-WT and *HAC701* mutant lines, *9-5*$^{-/-}$, *9-12a*$^{-/-}$, and *9-12b*$^{-/-}$ with mock (10 mM $MgCl_2$) and *Pseudomonas syringae* pv. *oryzae* (*Pso*) (OD = 0.2; resuspended in 10 mM $MgCl_2$) for 72 h. *Pso* is a causative agent of halo blight in rice characterized by brown lesions and yellow halo-like blotches on leaves (25). Infection of *Pso* showed that *hac701* was resistant to *Pso*-treatment as compared to 9-WT (Fig. 1C; Fig. S3). These data suggest that *HAC701* might be involved in the regulation of rice innate immunity acting in its capacity as a transcriptional coactivator and/or as an acetyltransferase. We further tested whether *hac701*

158 also shows resistance phenotype when infected with a rice blast pathogen, *Magnaporthe*
159 *oryzae*. Although the data were not statistically significant, results showed a resistant
160 phenotype tendency in *hac701* (Fig. 1D). Overall, these indicate that *HAC701* plays a negative
161 role in rice innate immunity.

162 **Transcriptome profiling of the rice-*Pso* pathosystem.**

163 To profile the genome-wide effect of *HAC701* mutation in rice innate immunity, we performed
164 RNA-sequencing on mock- and *Pso*-treated 9-WT and *hac701* using local leaf tissues (Fig. S4;
165 Table S2). We first characterized the effect of *Pso* infection on 9-WT and analysis of the highly
166 variable genes in mock- and *Pso*-treated 9-WT plants showed gene clusters that were
167 dependent on *Pso* induction alone (Fig. S4; Fig. S5). The top 10 highly variable genes across
168 the 9-WT samples showed features involved in tolerance and/or resistance such as disease
169 resistance and stress tolerance mostly by catalysis of primary and secondary metabolism (Fig.
170 S5). This includes well-documented genes involved in plant resistance against pathogens, such
171 as tryptophan decarboxylase 1 (Os08g0140300) that catalyzes the production of serotonin via
172 conversion of tryptophan to tryptamine in rice (26), which has been implicated to confer
173 resistance in rice infected with *Bipolaris oryzae* (27). Another gene, naringenin 7-O-
174 methyltransferase (Os12g0240900), that catalyzes the production of rice phytoalexin
175 sakuranetin has been reported to participate in rice defenses via JA signaling (28, 29). Lignin
176 and phytoalexin encoding genes for instance laccases (*e.g.* Os12g0258700, Os11g0641500)
177 and cytochrome P450s (*e.g.* Os07g0218700, Os08g0508000) are metabolic products known to
178 be involved in plant defenses as well (30-32). Gene Ontology (GO) analysis of upregulated
179 genes in *Pso*-infected 9-WT plants revealed enrichment of genes involved in response to biotic
180 stimulus (GO terms: Response to wounding, Response to other organism, Cell wall
181 macromolecule catabolic process, *etc.*) (Fig. S6; Table S3). Both up and downregulated genes
182 showed enrichment of transcriptional machinery regulation, a possible consequence of

183 defense-related transcriptional reprogramming processes during bacterial invasion. GO
184 analysis also identified pathways associated with upregulated gene networks involved in plant
185 defense such as diterpene phytoalexin biosynthetic pathway and chorismate biosynthesis.
186 Thus, the rice-*Pso* pathosystem is a functional system to analyze defense responses of rice
187 against *Pso* infection.

188 **Potentiated *WRKY45* gene in *hac701* provides resistance against *Pseudomonas* and**
189 ***Magnaporthe* infections.**

190 To investigate the molecular basis of resistance phenotype observed in *Pso*-infected *hac701*,
191 we further analyzed our transcriptome data and found 141 upregulated genes in *hac701* (Fig.
192 S7A; Table S4). We refer to these genes as *HAC701*-repressed genes. GO analysis of *HAC701*-
193 repressed genes showed enrichment of processes involved in response to xenobiotic stimuli
194 and defense response (GO terms: Response to xenobiotic stimulus, Response to wounding,
195 Regulation of defense response, Jasmonic acid mediated signaling pathway, Defense response,
196 *etc.*). These genes were lowly expressed in the 9-WT background. On the other hand, 336
197 upregulated genes in the 9-WT background alone referred to as *HAC701*-independent genes
198 did not show a very distinct enrichment of genes in defense responses yet rather showed a more
199 general biological and physiological processes (GO terms: Mitochondrial respiratory chain
200 complex IV assembly, Alanine transport, Cellular response to heat, *etc.*) (Fig. S7A; Table S3).
201 We also looked into the features of 31 downregulated genes in the mutant background referred
202 to as *HAC701*-enhanced genes (Fig. S7B; Table S4). These genes were not normally
203 downregulated in the 9-WT background. *HAC701*-enhanced genes contained genes enriched
204 in photosynthetic and response to abiotic stress terms (GO terms: Glycerolipid biosynthetic
205 pathway, Response to cold, Photosynthesis, *etc.*). In addition, the remaining 46 downregulated
206 genes in the 9-WT background alone also showed a more general biological processes with no

hint of enrichment in defense response against pathogen infection (GO terms: Chloroplast organization, Gluconeogenesis, Organelle fission, *etc.*) (Fig. S7B; Table S3).

We were intrigued what genes were affected in *HAC701* mutant background without *Pso*-treatment. Thus, we analyzed the transcriptome of mock-treated *hac701*, and found a small number of DEGs (98 genes; Table S5) mainly enriched in NADH dehydrogenase complex assembly and photosynthesis. This is in contrast with the number of DEGs found in *Pso*-treated *hac701* transcriptome, which yielded 660 genes (Table S6). These results simply indicate that *Pso* induced the expression of substantial number of genes in *hac701*. To fully understand the role of *HAC701* in *Pso*-treated conditions, we overlapped the list of genes derived from mock and *Pso*-treated mutants, and found *WRKY45* (*OsWRKY45*) upregulated in the *hac701* background in mock-treated *hac701* (Fig. 2A). *WRKY45* was also identified as one of the 141 upregulated genes in *Pso*-infected *HAC701* mutant (Fig. S7A). There was no candidate gene found downregulated in *HAC701* mutant background alone (Fig. 2A). We then checked whether there were differences in the upregulation strength of *WRKY45* in the *HAC701* mutation alone, compared to *HAC701* mutation combined with *Pso*-treatment. Transcriptome data revealed that *WRKY45* expression was increased by about 20% upon *Pso*-treatment (Fig. 2B). These results suggest that *WRKY45* expression is partially dependent on *HAC701* mutation. In addition, *Pso*-treatment allowed the co-expression of genes downstream of *WRKY45* pathway in a HAC701-dependent manner.

hac701 phenocopy _WRKY45_ overexpression transgenic plants.

To determine whether the upregulation of *WRKY45* in *hac701* is relevant to rice with overexpressed *WRKY45*, we compared the DEGs in our *hac701* with *WRKY45* overexpression (*WRKY45-ox*) lines previously reported (in these studies: 33, 34). Our results indicated a striking similarity of targeted genes from rice samples despite the fact that they were inoculated

with two different types of pathogens, a bacterial (*Pso*; this project) and the fungal pathogen *Magnaporthe* (33, 34) and minor differences in sampling time periods (Fig. 3). In addition, we then analyzed whether benzothiadiazole-responsive genes (Fig. 3A; Table S6; Table S7) would overlap with *HAC701* mutant-DEGs in *Pso*. It is known that benzothiadiazole (*i.e.* BTH is a synthetic analog of salicylic acid, SA) robustly induces defense genes in rice (34, 35), which usually contains high levels of SA. As a result, about 43.3% (286/660 genes; $P<3.336e-161$) of *HAC701* mutant-DEGs in *Pso* overlapped with BTH-responsive genes, while about 12.4% (82/660 genes; $P<2.368e-79$) of the *HAC701* mutant-DEGs in *Pso* overlapped with BTH- and WRKY45-regulated genes (Fig. 3B; Table S8). Furthermore, genes upregulated in plants expressing DEX-induced myc-tagged WRKY45 protein in rice were mostly found in *HAC701* mutant-DEGs in *Pso* (75% or 9/12 genes; Table S9). Our analysis also showed that at most 9.1 % (60/660 genes; $P<3.986e-15$) of the *HAC701* mutant-DEGs in *Pso* were regulated in BTH- and NPR1/NH1-dependent manner (Fig. 3B; Table S10). The rice NPR1/NH1 is an independent immune signaling pathway that mediates gene responses through BTH/SA-induction (Fig. S18). We then analyzed the 72 *HAC701* mutant-DEGs in *Pso* that were exclusively regulated by BTH- and WRKY45 as well as the other 10 genes jointly regulated by WRKY45 and NPR1/NH1 under BTH treatment (Fig. 3B-D). We found that most of these *HAC701* mutant genes were genuine WRKY45-regulated genes (Fig. 3C-D) (33, 34). Analysis of these WRKY45-dependent defense-related genes showed that in the presence of *Pso*-infection, a number of glutathione-S-transferase (GST) gene, were more upregulated in 9-WT than in *hac701* (Fig. 3D). These results were also consistent with the result that *OsWRKY62*, a known negative regulator and direct target of *OsWRKY45* (34), had lower transcription level in *HAC701* mutants (Fig. 3D). It is interesting that genes in JA biosynthesis, signaling and perception tend to be more highly expressed in *HAC701* mutant than 9-WT (Fig. 3D). In addition, *HAC701* mutant genes that were found regulated in BTH and *WRKY45* indeed

contain W-box motifs (i.e. binding motifs for WRKY transcription factors, 36), raising more the possibility that these genes are direct WRKY45 targets (72/82 or 87.8%; Table S11). Meanwhile, all 10 genes that were commonly regulated in BTH, *WRKY45*, and *NPR1/NH1* (Fig. 3) contain W-box motifs as well (10/10 or 100%; Table S12). Taken together, these results indicate that upregulation of *WRKY45* expression as an outcome of *HAC701* mutation resulted in expression profile of genes almost identical to overexpressing *WRKY45* transgenic lines as well as to DEX-inducible *WRKY45* expression system. These also suggest that a significant fraction of *HAC701* mutant DEGs are probably WRKY45-regulated, given the presence of W-box motif.

Surprisingly, the upregulation of *WRKY45* expression in *hac701* did not result in any visible morphological defects (Fig. S1G). This indicates that *WRKY45* does not pose growth penalties, at least in this case where there is no pathogen applied.

WRKY45 promoter contains CRE motif.

Rice HAC701 and two others, HAC703 and HAC704, belong to the CBP [Cyclic adenosine monophosphate response element-binding protein (CREB) Binding Protein] family group of proteins that is known to bind CREB transcription factor through its KIX domain (7, 37). Therefore, we examined *in silico* the members of rice CBP family for the presence of KIX domains using a KIX domain database (38). Our results showed that only HAC701 and HAC703 proteins contain the highly conserved KIX domain (Fig. S8). Although we have not identified CREB-like transcription factor candidates in rice so far, we further examined the DNA motifs in the 1kb promoter regions of the 660 *HAC701* mutant-DEGs in *Pso* that might potentially bind to KIX-CREB-like transcription factor. Our DNA motif analyses result showed 49 significantly enriched motifs in promoters (Table S13; E-value <0.05). We then used these motifs to compare against a database of known motifs and found a CRE motif when

the query sequence CGRCGRCG (E-value<1.5e-27) was used (Fig. S9A). The CRE motif is a well-known sequence motif in animals usually bound by KIX-CREB transcription factor complex (39). We then searched for genes that contain the CRE motif and found that only five genes (0.76%) contain full CRE motif (Fig. S9B; Table S6). To our surprise, *WRKY45* promoter contains the full CRE motif that could possibly be targeted via KIX domain and CREB-like transcription factor-dependent regulation in rice system (Fig. S9C). These data show that *WRKY45* promoter could possibly be *cis*-regulated by HAC701 through its KIX domain, while the occurrence of CRE motif is not necessarily associated with other HAC701-regulated genes.

Genome-wide investigation of histone modifications and enriched gene targets in *HAC701* mutant.

The CREB-binding protein (CBP) is also known to regulate gene expression by acetylating histone tails in both animals and plants (40). Thus, we performed chromatin immunoprecipitation coupled to sequencing (ChIP-seq) analysis on histone markers associated with active and repressive chromatin to examine the landscape of chromatin modifications in *HAC701* mutant. We performed ChIP-seq analyses of H3K9 acetylation (H3K9ac), H3K27 acetylation (H3K27ac), H3K9 di-methylation (H3K9me2), and H3K9 tri-methylation (H3K9me3) on untreated 9-WT and *9-12b*$^{-/-}$ mutant (Fig. S10; Table S14). Metaplot profiles of these histone modifications were generated for genes, transposable elements (TEs), and simple repeats (Fig. S11; Fig. S12). The enrichment profiles show that both H3K9ac and H3K27ac accumulated in genes mainly along the transcriptional start site (TSS) and tapering through the gene body regions. In contrast, we found that H3K9me2 and H3K9me3 were highly depleted in the gene TSS region (Fig. S11A). As expected, H3K9 and H3K27 acetylation marks were depleted in TEs, while H3K9 di- and tri-methylation marks showed enrichment (Fig. S11B). In addition, enrichment analysis of simple repeats showed similar profiles with TEs in both

acetylation and methylation histone marks, although simple repeats tend to be highly enriched in H3K9me2 at a narrow set of genomic loci (Fig. S12). These results showed that our ChIP-seq profiles of histone modifications were largely consistent with the previous report on rice ChIP-seq analysis (41).

The observed low enrichment of H3K9ac in *9-12b*$^{-/-}$ mutant is a probable indication of mutation on *HAC701* gene (Fig. S11A). Therefore, we further analyzed the significantly enriched or depleted regions in *9-12b*$^{-/-}$ by taking the enrichment ratio of 9-WT over *9-12b*$^{-/-}$ (wild type/*hac701*) in H3K9ac, H3K27ac, H3K9me2, and H3K9me3 modifications. These analyses yielded 265 peaks in the H3K9ac fraction (Fig. 4A; Table S14). From the metaplot analysis, it showed that *9-12b*$^{-/-}$ has depleted H3K9ac enrichment in the 265 regions identified containing putatively 263 genes (Fig. 4A; Table S15), which include *HAC704* and *HAC701* loci and a mediator gene, *MED11* (Fig. 4D; Fig. S13A). These 265 regions were not associated with changes in other modifications in *9-12b*$^{-/-}$ mutant when compared to 9-WT (Fig. 4B). These results suggest that HAC701 acetyltransferase may have a specificity to H3K9 site. It also suggests that HAC701 probably autoacetylates its own promoter including another member of CBP family, *HAC704*.

We then analyzed the GO enrichment features of the putative 263 genes found in these 265 regions with H3K9ac changes (Fig. 4C; Table S15). The results indicate that these genes function in processes involved in the flow of genetic information, DNA methylation in the CHH-context, circadian rhythm, organellar transport, cell cycle and reproduction, ubiquitination, and in a number of biosynthetic processes. It is also perhaps not surprising that histone acetylation was also enriched. In addition, enrichment of genes involving environmental responses included heat stress and innate immunity were observed, in which about 9% (23/263) were possibly involved in defense responses. A large fraction of these defense genes were identified as candidate sensors or decoys (e.g. Cyclin A1, Thioredoxin,

Jacalin-like lectin, *etc.*) that may act as negative regulators of rice effector-triggered immunity (ETI-immunity) (42) (Fig. 4E; Fig. S13B). The distribution of these 265 regions in H3K9ac ChIP revealed that a large portion were found in genes (73.58%) followed by promoters (18.11%) (Fig. S14). It is also interesting to note that H3K9ac in these identified regions was found in transposable elements (7.55%). Overall, these results demonstrate that HAC701-dependent acetylation of H3K9 histone site might modulate transcription of decoy genes that are monitored by R proteins in rice immunity. Additionally, H3K9ac assessed in different regions of the rice genome showed that it is found mostly in genes and promoters with high similarity in the previous study (41).

We proceeded by analyzing the general distribution of H3K9ac, H3K27ac, H3K9me2, and H3K9me3 peaks in intergenic and intragenic regions of rice genome in 9-WT and *9-12b*$^{-/-}$ mutant (Fig. 5A). A large proportion of H3K9ac and H3K27ac were concentrated on exonic and intronic regions of the gene, while *HAC701* mutation resulted in the increase of enrichment of H3K27ac genome-wide on all regions of the rice genome (Fig. 5A). It is also worth mentioning that loss of *HAC701* increased the level of enrichment of these methylation modifications in intergenic regions. These data suggest that the loss of *HAC701* leads to an increase of a counter acetylation modification, H3K27ac, on a genome-wide scale.

To explain the disease resistance phenotype of *hac701* through WRK45-dependent immune pathway, we investigated the genomic locus of rice *WRKY45* (Fig. 5B). The upregulation of WRKY45 was accompanied by H3K9ac enrichment along the 1kb upstream region of *WRKY45* gene in *9-12b*$^{-/-}$ (Fig. 5B, C). As the CRE motif was specifically enriched in the promoter region of *WRKY45* (Fig. S9C), we compared the enrichment of H3K9ac and H3K27ac in *9-12b*$^{-/-}$ *WRKY45* promoter. We found that H3K9ac, but not H3K27ac, was highly enriched in this regulatory region (Fig. S15), while H3K27ac of *WRKY45* gene body was less pronounced than H3K9ac. Overall, our ChIP-seq data are consistent with RNA-seq data in

355 showing that mutation in *HAC701* gene potentiated *WRKY45* locus by regulating the
356 enrichments of histone acetylation and methylation modifications on *WRKY45* promoter. We
357 also found that the CRE motif of *WRKY45* is modulated by H3K9ac and perhaps other
358 modifications, including those that are analyzed here.

359 **Systemic gene expression in rice-*Pso* pathosystem.** To explore the nature of systemic gene
360 expression in rice-*Pso* pathosystem, we performed RNA-sequencing on systemic or distal
361 tissues of 9-WT and *hac701*. The tissue samples were collected together with infected samples
362 (local samples) 72 hours after *Pso* infection without further bacterial treatment. Genome-wide
363 transcriptome analysis in systemic 9-WT samples showed that 24 genes were differentially
364 expressed, and among them were eight genes that were common to both local and systemic
365 tissues (Fig. S16A; Table S16). Comparative analysis also showed that although there were
366 substantial expression changes in systemic tissues, the number of DEGs was highly reduced in
367 systemic tissues than in local tissues. Among the eight DEGs, five of them showed altered
368 transcriptional expression from local to systemic tissues (Fig. S16B). These genes were
369 mannose-specific jacalin-related lectin/*OsJAC1* (Os12g0247700) (43), putative cytochrome
370 P450 (Os09g0275400) (44), ATPase (Os07g0187400), GDP-L-galactose phosphorylase
371 (Os12g0190000) (45), and terpene synthase (Os04g0344100), some with putative functions in
372 response to pathogen infection or stress. These results indicate that these genes were mostly
373 activated locally in the infection site and that any altered expression in distal tissues may
374 facilitate systemic form of resistance. To compare the effect of *HAC701* mutation on the
375 number of DEGs, we analyzed the MA-plots of systemic tissues of 9-WT and *hac701*. Our
376 results showed that the number of DEGs with significant expression (*i.e.* those that are in red)
377 was diminished in the mutant background implicating a possible role of *HAC701* in systemic
378 signaling in rice-*Pso* pathosystem (Fig. S17). Overall, these results indicate that systemic
379 tissues in *Pso*-challenged 9-WT plants have augmented transcriptional gene expression that

possibly aims to potentiate distal tissues on the onset of secondary pathogen attack. This also indicates that *HAC701* might potentially regulate systemic defenses through an unknown mechanism at distal non-infected site in preparation for future infection episodes.

DISCUSSION

Histone acetyltransferases or HATs and their complexes are involved in various biological processes in the cell. Currently, studies have been focused on the roles of HATs specifically members of the CREB-binding protein (CBP) family in regulating substrate specificity and enzymatic activity such as acetylation (40). However, its involvement in molecular signaling pathway leading to modulation of plant immunity remains to be explored. Therefore, it is expected that the analysis of plant CBP will facilitate a broader understanding of regulation of gene expression and protein function in plant immunity pathways.

In this study, we generated CRISPR/Cas9 mutants of the rice *HAC701* gene, a member of the CBP family of HATs, since our results indicated its involvement in rice immunity. By inoculating a rice compatible bacterial pathogen, *Pseudomonas syringae* pv. *oryzae* (*Pso*), we showed that *hac701* are resistant to *Pso* proliferation and also showed resistance tendency when infected with *Magnaporthe* (rice blast). These indicates that *HAC701* negatively regulates rice immunity responses to *Pso* and *Magnaporthe* pathogens. When we analyzed our transcriptome data, it showed that this negative regulation of immunity by *HAC701* is attributable to suppression of a major immunity pathway in rice probably through WRKY45. In *hac701*, *WRKY45* gene expression is upregulated and it seemed to be in a potentiated state enabling a further increase of expression upon bacterial infection. In addition, both morphological phenotypes and target genes in *hac701* mimic those in *WRKY45-ox* transgenic lines possibly indicating a genetic interaction of *HAC701* and *WRKY45* genes. Lastly, we showed in our ChIP-seq analysis that the promoter of *WRKY45* in *hac701* is enriched in

405 H3K9ac coinciding with a *cis* regulatory CRE motif that might be responsible for *WRKY45*
406 upregulation and control.

407 In Arabidopsis, the p300/CBP acetyltransferase gene, *HAC1*, has been shown to
408 positively regulate defense priming only in repetitively abiotic-stressed plants (46). *hac1-1* did
409 not show any immunity related responses prior to abiotic stress applications indicating that
410 Arabidopsis *HAC1* requires several abiotic stress stimulations to activate its immunity.
411 However, this is not the case in *HAC701* in rice. We showed that the rice *HAC701* did not need
412 abiotic stress stimulation to be transcribed and to effect pathogen and disease specific
413 phenotypes (Fig. 1; Fig. S2; Fig. S3). Rather, our results are consistent with the disease
414 phenotype exhibited by Arabidopsis mutant of GCN5, an acetyltransferase member of the
415 SAGA transcriptional coactivator complex catalyzing the H3K14 modification site and at the
416 same time influencing the acetylation of H3K9 (47). The *gcn5* showed upregulation of SA-
417 mediated immunity resulting in resistance against *Pseudomonas syringae* pv. *tomato* infection.
418 In our study, we found that WRKY45-dependent pathway confers resistance to *hac701*.
419 Consistent with the view that the rice hormone defense network does not support a
420 dichotomous role of salicylic acid (SA) and jasmonic acid/ethylene (JA/ET) phytohormones in
421 regulating rice immunity (48), we found no evidence in this study that SA-mediated immunity
422 played a central role in *hac701* resistance phenotype. However, we found JA-related
423 differential gene expression as components of WRKY45-dependent defense-related genes
424 (Fig. 3D). Indeed, JA biosynthesis is known as a downstream target of rice WRKY45 (49). In
425 rice immunity model, both SA and JA/ET are considered effective in defense responses against
426 (hemi) biotrophic and necrotrophic pathogens (48, 50, 51). While SA-mediated *AtNPR1*
427 regulates majority, if not all, of Arabidopsis immune responses (52), *OsWRKY45* and
428 *OsNPR1/NH1* are mostly independent of each other (34; Fig. S18). Although, our results
429 suggest that *hac701* DEGs partially overlapped with NPR1/NH1-dependent pathways (Fig.

3B). Given that the rice system has a constitutive high levels of SA compared to most plants including Arabidopsis and tobacco, and pathogen applications did not increase its basal SA level (53, 54), our results are consistent with this report that SA in rice may not directly act on pathogens, rather, it may function to potentiate endogenous defense pathways in which *WRKY45* plays the central role. *OsWRKY45-ox* showed strong resistance against blast pathogen, even though lacking the constitutive expression of defense genes prior to blast infection (34). It could be that disruption of HAC701-dependent pathways through *HAC701* mutation led to activation of WRKY45-dependent pathways in an already SA-potentiated rice network, although this needs to be further examined in detail. Our results are also consistent with the disease phenotype presented by non-sense mutation in *Med15* gene, a subunit of Mediator complex (55). The *med15b.D* wheat mutants were resistant to stem rust, and the authors attribute a part of this to segmental coregulation in which a certain portion of the chromosome containing R genes (i.e. specifically NLR) was differentially expressed in wild type compared to mutant. While we did not observe any form of segmental coregulation in our analysis of *hac701*, we found that mutations in *HAC701* resulted in downregulation of ETI components notably the decoys/sensors (Fig. 4E).

OsHAC701, *AtHAC1*, *AtGCN5*, and *TaMed15*, play a central role in regulating the transcriptional machinery. They likely do this regulation by associating themselves and their complexes to RNA polymerase II and transcription factors as shown by their homologous counterparts in animals (4, 14, 56, 57). This is possible because they are multidomain genes that have the capacity to form and maintain large complexes. Os*HAC701*, *AtHAC1*, and *AtGCN5* are also involved in regulating abiotic stress responses suggesting that the complexity and specificity of their activities are dependent on their interacting factors that recruit them to the biological pathway itself (6, 7). Furthermore, majority of these genes, *OsHAC701*, *AtHAC1*,

454 and *TaMed15*, encode the KIX domain, a docking site for transcription factors reported to be
455 involved in plant immunity (58).

456 In line with the above results, we propose that HAC701 is a negative regulator of
457 WRKY45-dependent defense pathway in rice (Fig. S18). We suggest here two possible
458 mechanistic insights into HAC701 regulation of WRKY45 that need further experimental
459 evidence. First, similar to Med15, the HAC701-mediated immunity may require a loss or
460 truncation of HAC701 in regulating the transcription of *WRK45* locus. Given that the promoter
461 of *WRKY45* contains a rare CRE motif (Fig. S9), we assume that an unidentified CREB-like
462 transcription factor with regulatory potential is interacting with HAC701 through its KIX
463 domain (Fig. S8) and with the CRE motif of *WRKY45* promoter. This interaction may also
464 include other protein interactors specific to *WRKY45* locus regulation. From our results,
465 mutation of *HAC701* is enough to potentiate *WRKY45* and further addition of *Pso* enables
466 *hac701* to mount higher *WRKY45* expression compared to 9-WT. These suggest to us that
467 *WRKY45* locus is poised for activation as suggested by our ChIP-seq analysis of untreated
468 *hac701* (Fig. 5). However, the H3K9 acetylation we observed in *WRKY45* promoter might not
469 be catalyzed by HAC701 itself in *hac701*, but may come from other CBP family members (Fig.
470 1A; Fig. S1H) or other HATs. Although, we do not have ChIP-seq data for pathogen inoculated
471 *hac701*, our RNA-seq data suggest that the poised *WRKY45* through *HAC701* mutation is
472 enough to activate downstream defense likely through *WRK45*-dependent signaling. Second,
473 the decoys/sensors component that we found may act as negative regulators as predicted by the
474 Decoy model (Fig. 4E) (42, 59). It could be that HAC701 maintains the acetylation of these
475 decoys/sensors to equilibrium. Any disturbance in their expression could possibly lead to
476 activation of R genes monitoring these decoys/sensors, which could in effect activate
477 WRKY45-dependent immunity. Indeed, we found seven R genes upregulated in *HAC701*
478 mutation treated with *Pso* (Table S17). It is of course possible that these two mechanisms are

479 occurring simultaneously in conferring resistance, although finer details of these proposed
480 mechanisms are still unknown.

481 As HAC701 is a global transcriptional regulator, we found that it regulates a myriad
482 number of biological processes underscoring its importance in genome and epigenome control
483 (Fig. 4C). Among the enriched GOs, we found histone acetylation and innate immune
484 responses were affected in *hac701*. These suggest to us the intricate network in HAC701-
485 dependent regulation of immunity through its scaffolding and catalytic activity in the cell. It is
486 possible that any misregulation in *hac701* could lead to genome-wide functional compensation
487 events by activating other proteins acting on the same pathway as HAC701. This compensation
488 functionality has been shown in a PHD-finger protein, Enhanced Downy Mildew 2 (EDM2),
489 in NLR (i.e. a type of R protein) protein expression control as it affects plant fitness (60).
490 Therefore, it is also likely that the expression regulation of *WRKY45* locus as well as the
491 decoys/sensors may be subjected to compensatory regulation in the case of *HAC701* mutation.

492 The heterochromatic marker, H3K9me3, is common in animals, but rarely found in
493 Arabidopsis and in plants in general (61). Indeed, our analysis did not find the peaks in 9-WT
494 ChIP-seq, although we found 33 peaks in the *HAC701* mutant (Table S14). Most H3K9me3
495 enrichments were found in intergenic regions and in only two genes with intragenic
496 enrichments. Table S18 also shows genes nearest the H3K9me3 enrichment in the intergenic
497 regions. These results suggest that H3K9me3 is maybe a rare modification and is possibly
498 modulated by HAC701 presence and activity in certain genomic regions.

499 Trade-off between growth and defense in plants is a common occurrence and often
500 considered inevitable (62, 63). However, we were surprised to find that *hac701* in the T2 up
501 until T4 generations do not have readily visible penalties in height, tiller number, number of
502 effective grains, and grain weight (Fig. S1D-I). Previous studies showed that *WRKY45-ox* had

503 no obvious autoimmunity phenotype, although there was a slight decrease in height observed
504 as compared to wild type in response to growth conditions (33, 34). In this study, WRKY45-
505 dependent resistance against *Pso* was observed in *hac701* (Fig. 1C, Fig. S3). Furthermore, these
506 *HAC701* mutants also showed resistant tendencies against *Magnaporthe* infection (Fig. 1D).
507 *WRKY45-ox* treated with *Magnaporthe* showed resistance, while a BTH-induction in
508 knockdown *WRKY45* mutants did not rescue the *Magnaporthe* resistance and remained
509 susceptible (34). Together these suggest that morphological and disease phenotypes of *hac701*
510 resembled that of *WRKY45-ox* indicating that *HAC701* mutation indeed upregulates *WRKY45*
511 gene that prompts WRKY45-dependent defense pathway into action leading to resistance
512 against bacterial and fungal pathogens. It could be that the potentiated state of *WRKY45* in
513 *hac701* has modulated the expression of resistance from affecting these agronomic traits.
514 Nonetheless, the mechanistic basis for this trade-off, if it truly exists, is not well understood
515 and needs further investigation.

516 We would like to emphasize that at the moment we do not have strong evidence that
517 HAC701 specifically catalyzes H3K9 acetylation. Although, the H3K9ac antibody used in this
518 study detected H3K9ac decrease of numerous loci in *hac701* compared to 9-WT that are not
519 present in H3K27ac, histone target-specificity of HAC701 still needs to be verified. As
520 H3K9ac and H3K14ac were seemed co-regulated and were directly correlated to each other in
521 regulating their common target genes (47), we assume that the H3K14ac in our *hac701* would
522 show the same correlation as well.

523 HAC701 appears to be an ancient protein in the CBP histone acetyltransferase family
524 clade (Fig. 1A). The fact that *HAC701* mutation is not lethal, suggests that other CBP members
525 and arguably members of other histone acetyltransferase families might have redundant
526 functions at some regulatory level. However, our results showing that *hac701* has enhanced
527 disease resistance phenotype and reduction in acetylation demonstrate certain functional

528 specificities through HAC701-dependent pathways. Also, the fact that *hac701* showed
529 reduction in expressed genes at the systemic level (Fig. S17), indicates possible broader roles
530 of HAC701 other than localized modulation of rice innate immunity.

531

532 **MATERIALS AND METHODS**

533 **Biological samples and plant growth conditions**. *Oryza sativa* ssp. *japonica* cv. Nipponbare
534 (wild type) plants and mutant lines were grown in commercial soil (Kumiai, JA Okinawa) at
535 30°C day/25°C night temperatures under a 12-h-light/12-h-dark photoperiod in an incubator
536 (BiOTRON, NK System). The lighting was supplied by white light at an intensity of 31,000
537 lx. Relative humidity was at 70%. For embryonic rescue, rice embryos were extracted from
538 wild-type immature seeds 10-14 days after flowering. Embryos were grown into plantlets in
539 Murashige and Skoog (MS) agar medium before being transferred to soil for further growth.

540 **Isolation and screening of *HAC701* mutant lines**. To generate *HAC701* CRISPR/Cas9
541 knockout mutant lines, two sgRNA *HAC701*-specific target sites were obtained from CRISPR-
542 P website and were used to synthesize primers for pRGEB31 (stable system) (64) (Table S1).
543 Briefly, the vectors were digested with BSA I, while primers were phosphorylated and
544 annealed to produce a DNA oligo duplex. The digested vectors were ligated to DNA oligo
545 duplex using T4 ligase. CRISPR/Cas9 vectors were introduced into *Agrobacterium* EHA105
546 and rice calli were transformed using the standard *Agrobacterium*-mediated transformation
547 procedure. For CRISPR/Cas9 T0 and T1 screening, leaf samples were collected and genomic
548 DNA was extracted using a standard CTAB protocol. Then, PCR-RFLP assay utilizing BseLI
549 restriction enzyme (Thermo Fisher Scientific) was used to detect the CRISPR/Cas9-engineered
550 mutations on *HAC701* targets (Table S1). Positive lines detected by PCR-RFLP assay were
551 further analyzed by sequencing for INDEL mutations using S2 and S5 forward primers (Table

S1). Four DNA amplicons per line were cloned and sequenced to determine the zygosity of the lines. Biallelic mutations were found in a few T0 and T1 lines. First exon (Target 1) was initially targeted in *HAC701* gene using a CRISPR/Cas9 vector construct containing a single-guided RNA (S2) (Fig. S1A; Table S1). The isolation of the first generation (T0) *CRISPR Cas9-HAC701-S2* lines yielded 90 positive independent lines, and among these, randomly chosen representative lines were further genotyped to characterize the identified DNA mutation. PCR and RFLP assays resulted in the isolation of monoallelic lines characterized mostly by deletions and a few insertions (INDELS) on or surrounding the targeted site of sgRNA (S2) (Fig. S1B-C; Table S1). The T1 *HAC701-S2* generation as observed from seeds showed conservation of mutation directly from parental lines (Fig. S1B). Then, mutant lines were isolated using the same technology targeting the fifth exon (Target 2) of the *HAC701* gene using a construct that also contains a single guide RNA (S5) (Fig. S1D; Table S1). The *CRISPR-Cas9-HAC701-S5* (T0) lines generated 11 positive independent lines of which three were genotyped for verification of mutations (Fig. S1E). Second generation (T1) lines also showed conservation of mutations (Fig. S1E). Similar to *HAC701-S2* lines, genotyping showed INDELS in proximity to or on the target site.

Phenotyping. Positive lines containing biallelic homozygous mutations were phenotyped for effective grain production by examining and counting the mature grains produced in each panicle. Tiller number was counted one month after flowering. Chlorosis phenotype was used as a proxy for any defect in photosynthesis and or apparatus. 1000-grain weight was measured on seeds oven dried for 30-days at 37°C. Comparison of height and general morphological structures were documented using photography.

flg22 leaf disc assay. flg22 peptide, a well-known inducer of plant innate immunity, specifically of PTI was used to test which rice HATs respond to flg22 treatment. Leaf disc assay (modified from 65, 66) was performed on fully expanded 30-d-old wild-type leaf samples

and treated with synthetic flg22 peptide (30-51 aa, Flic, *Pseudomonas aeruginosa*) (ADI, Inc.) at different time periods and concentrations. Briefly, leaves were cut into about 5 mm sizes and floated on the water for 24-h in growth chamber to remove the symptoms of wounding stress. Leaves were then treated with PAMP solution in water at 15 ml falcon tubes with rotation (Corning Science). After treatment, paper towel-dried leaves were frozen in liquid nitrogen.

Pathogenesis assay. Seeds were surface sterilized and imbibed in sterile water in the dark for 72 h before sowing on MS basal medium (Sigma Life Science). After 10 days, the plantlets were transferred to soil and were grown for another 18 days until infection. *Pseudomonas syringae* pv. *oryzae* (*Pso*) (MAFF No. 301530, NIAS Genebank) was grown in Luria-Bertani (LB) broth (Sigma-Aldrich) at 28°C until OD = 0.2 and was resuspended in 10 mM $MgCl_2$. The fourth leaf counting from the first true leaf was infected with *Pso* using needleless syringe injected from the lower surface of the leaf. *Pso* leaf infiltration was performed 10 cm from the tip of the leaf and was done 3x with approximately 1 cm space between the infiltration sites. Infected plants were temporarily maintained outside the growth chamber for 2 h to allow drying of the infected sites before returning to the chamber. Infected leaf samples were collected 3 days after *Pso* inoculation utilizing only the tissues comprising the spaces between the infiltration sites. These tissues were grounded in sterile 10 mM $MgCl_2$ and the grounded tissue suspensions were transferred to LB agar medium for incubation. The infected local tissues were assayed with minor modifications as detailed in Liu*, et al.* (67). For log cfu per leaf disc measurement, the grounded tissue suspensions were serially diluted six times to be able to count with accuracy the *Pso* colonies on Luria-Bertani (LB) agar medium. *Pso* colonies were counted from 4^{th} until 6^{th} serial dilution in several independent and genotypically dissimilar *hac701* lines*, 9-5*$^{-/-}$, *9-12a*$^{-/-}$, and *9-12b*$^{-/-}$. The remaining samples of the fourth leaf were used for RNA-sequencing analysis. For blast assay, the fifth leaf of 25-day-old plants were used for infection of *Magnaporthe oryzae* (MAFF No. 101511, NIAS Genebank). Blast spores were

602 incubated 10 cm from the tip of the leaf (1st site) and at another site of the same leaf 10 cm
603 from the first site (2nd site). Infected plants were incubated for 10 days inside an incubator
604 (BiOTRON, NK System) and the length of blast infection was measured.

605 **Gene expression analysis**. Total RNA extraction was performed using RNeasy Plant Mini Kit
606 (Qiagen) or Maxwell® 16 LEV Plant RNA Kit (Promega). cDNA was synthesized using
607 Primescript II 1st Strand cDNA Synthesis Kit (Takara) according to manufacturer's
608 instructions. RT-qPCR assays were performed on three biologically independent samples or
609 as indicated. RT-qPCR was performed using SYBR Premix Ex Taq II (Tli RNaseH Plus)
610 (Takara) and was calculated following Pfaffl (68) by averaging the values relative to *ACT1*
611 control gene. Primer sequences are listed in Table S19.

612 **RNA-sequencing**. Total RNA was isolated from mock- and *Pseudomonas syringae* pv. *oryzae*
613 (*Pso*)-treated 9-WT wild type and *hac701* with Maxwell 16 LEV Plant RNA Kit (Promega)
614 run on the Maxwell 16 Instrument (Promega) and/or mirVana miRNA Isolation Kit (Invitrogen
615 by Thermo Fisher Scientific). The *hac701* lines, *9-5*$^{-/-}$ and *9-12b*$^{-/-}$, were lumped together as
616 two independent biological samples during analysis. To remove the contaminating genomic
617 DNA from RNA samples isolated using the mirVana miRNA Isolation Kit, RNA was treated
618 with DNase I (RNA free) (Nippon Gene) following the manufacturer's instructions. Samples
619 were submitted to OIST Sequencing Center for RNA quality checking, library preparation, and
620 paired-end mRNA-sequencing (PE mRNA-seq).

621 **Chromatin immunoprecipitation-sequencing**.

622 ChIP analysis of histone modifications in wild type and mutants were performed as follows:
623 One-month-old mature leaves of wild type (9-WT) and *hac701* (*9-12b*$^{-/-}$) were fixed in a
624 fixation buffer (10mM Tris-HCl (pH 7.5), 50 mM NaCl, 0.1 M sucrose, 1 % formaldehyde)
625 for 10 min, followed by quenching with 125 mM Glycine for 5min. Nuclei isolation was

performed as previously described (69). Immuno-precipitation was performed for two replicates for each genotype (about 1 g tissue/IP) by SimpleChIP Plus Kit (Cell Signaling Technology) according to the manufacturer's instructions. Anti-Histone H3 antibody (Abcam ab1791), Anti-acetyl Histone H3K9 antibody (Merck ABE18), Anti-Dimethyl Histone H3K9 antibody (Merck 05-1249), Anti-Trimethyl Histone H3K9 antibody (Merck 17-10242), Anti-acetyl Histone H3K27 antibody (Abcam ab4729) were used for IPs. Dynabeads M-280 Sheep Anti-Rabbit IgG (Invitrogen 11203D) or Anti-Mouse IgG (Invitrogen 11201D) was used for purification of chromatin-antibody complex. Precipitated DNA samples were sequenced by Hiseq 4000 in 150 bp paired-end mode in OIST Sequencing Center. For ChIP real-time PCR, we used the "Percent Input Method" (Thermo Fisher Scientific) with 33% input value to normalize the data for enrichment calculation. Three independent biological replicates were performed for each sample.

Data analysis. For RNA-sequencing analysis, high quality reads were trimmed in order to remove sequencing bias and adapter effects. Trimmed reads were then mapped to the *Oryza sativa* spp. *japonica* genome (Os-Nipponbare-Reference-IRGSP-1.0) using Tophat (70, 71). Custom R scripts were used to generate the RNA count table necessary to analyze the differentially expressed genes (DEGs). Differential expression analysis was performed using DESeq2 package (72). DEGs were selected at Benjamini-Hochberg adjusted p value of < 0.01. To perform Gene Ontology (GO) analysis, gene lists were submitted to Enrichment Analysis (73) web tool of the Gene Ontology Consortium (74-76). To create the Venn diagram, gene sets were submitted to InteractiVenn web tool using *unions by list* to obtain overlapping components of input datasets (77). For ChIP-sequencing analysis, raw reads were trimmed and were mapped to *Oryza sativa* spp. *japonica* genome (Os-Nipponbare-Reference-IRGSP-1.0) using Bowtie (78). Read alignments were visualized using Integrated Genome Browser (IGB) (79). ChIP-enriched peaks were called by deriving a quantitative reproducibility score called

651 "irreproducibility discovery rate" (IDR) (73). Comparative analyses and quantitation of
652 enrichments between 9-WT and *hac701* (*9-12b*$^{-/-}$) were analyzed using a suite of tools and
653 utilities found in deepTools (80) and BEDTools (81). Peaks were positioned to genomic
654 locations (intergenic, genes, transposable elements, simple repeats) and within genes
655 (promoter, exon, intron, TSS, TTS). Table S14 showed the number of peaks identified for each
656 histone modifications in 9-WT and *hac701* (*9-12b*$^{-/-}$). Peak-to-gene assignment was performed
657 using Homer (v4.11) (82). To create the phylogenetic tree of Arabidopsis and rice histone
658 acetyltransferases, we used the UniProt amino acid sequences and reconstructed the
659 phylogenetic relationships using Phylogeny.fr (83, 84). For KIX domain analysis, we used
660 KIXBASE to perform multiple sequence alignment (38). To identify *cis*-elements on DNA
661 sequences, we used cister prediction software that utilizes hidden Markov model (85). For
662 motif analyses, we utilized the 1kb upstream promoter sequences of the sample genes. We used
663 Discriminative Regular Expression Motif Elicitation (DREME) (86) to discover the
664 significantly enriched motifs at a threshold of E-value<0.05 using shuffled input sequences as
665 control. These enriched motifs were used as query sequences in Tomtom (MEME suite 5.2.0)
666 to find similar motifs in published libraries. Libraries used were Eukaryotic DNA and
667 Vertebrates (*in vivo* and *in silico*).

668 **Data visualization**. Visualization of majority of the data was performed using Microsoft Excel
669 for Mac 2011 (version 14.7.1) and R packages: heatmaply, functions from *gplots*, and *ggplot2*.

670 **Data Repository**. For RNA-sequencing and ChIP-sequencing, raw data have been deposited
671 in the DDBJ Sequence Read Archive under accession ID (pending upon submission of data).
672 All other data can be found in the Supplemental Tables 1-19 in this manuscript.

673

674

675 **FIGURE LEGENDS**

676 **Figure 1** Disease phenotype of biallelic homozygous CRISPR/Cas9 lines targeting the fifth
677 exon of rice acetyltransferase gene, *HAC701*. (*A*) Phylogenetic relationships of members of
678 Arabidopsis and rice histone acetyltransferases. The numbers in red are branch support values.
679 All amino acid sequences are from UniProt database. (*B*) Upper panel: Alleles from four lines
680 of the second generation (T1) plants were identified by cloning and sequencing the PCR
681 products from *HAC701* target region using the primers found in Table S1. Lower panel: PCR
682 and RFLP assays of representative T1 generation lines. The mutant line *9-12a*$^{-/-}$ displaying a
683 wild type-like band was due to unaltered sequence order recognized by BseLI even after an
684 insertion event, however we confirmed by sequencing that an insertion mutation was present
685 in this line. (*C*) *Pseudomonas syringae* pv. *oryzae* (*Pso*) infection assay of *hac701*, *9-12b*$^{-/-}$ and
686 *9-5*$^{-/-}$ (T2), using *9-5*$^{+/+}$ segregated wild type line (9-WT) as control. Bacterial density
687 quantification uses values from 4th-6th serial dilutions. The mutant line *9-12b*$^{-/-}$ was grown from
688 the seeds of the third generation (T2), while *9-5*$^{-/-}$ line was embryonically rescued about 15
689 days post flowering from the second generation (T1) parental plants. All mock measurements
690 yielded zero bacterial growth for both wild type and mutant lines. Bars represent the 95%
691 confidence interval (CI) and compared to the wild type using two-tailed Student's *t*-test at
692 $P<0.05$ in *9-12b*$^{-/-}$; one-tailed Student's *t*-test at $P<0.05$ in *9-5*$^{-/-}$. (*D*) *Magnaporthe oryzae*
693 infection assay of *hac701*, *9-12b*$^{-/-}$ and *9-5*$^{-/-}$, using *9-5*$^{+/+}$ segregated wild type line (9-WT) as
694 control. Lesion length was measured on leaves after 10 dpi (days post infection). White length
695 indicator bar on the left panel is 10 mm. Bars on the right panel represent standard error (SE)
696 and compared to the wild type using *F*-test for variance and Student's *t*-test.

697

698 **Figure 2** The rice *WRK45* gene expression is induced in *hac701* lines. (*A*) Overlap analysis of
699 upregulated and downregulated genes in *hac701* background under mock and pathogen (*Pso*)-
700 treatment conditions (Table S5, S6). *OsWRKY45* is the only differentially expressed gene in
701 either the absence or presence of pathogen. Transcriptome data were normalized using mock
702 data sets for each genotype and condition. (*B*) *OsWRKY45* expression when *HAC701* is
703 mutated (+ sign). The addition of pathogen (+ sign) on *hac701* increased further the
704 *OsWRKY45* expression. Transcriptome data of *hac701*, *9-12b*$^{-/-}$ and *9-5*$^{-/-}$, under mock or *Pso*-
705 treated conditions were lumped as two independent biological samples for analysis (See Table
706 S2). hpi, hours after infection.

707

708 **Figure 3** *hac701* phenocopies *OsWRKY45* overexpression transgenic plants. (*A*) Overlap
709 analysis of differentially expressed genes (DEGs) in *hac701* background with benzothiadiazole
710 (BTH)-responsive genes (*i.e.* BTH is a salicylic acid analog) in wild type rice (Table S6, S7).
711 Significance value of the overlap data was tested using the hypergeometric distribution test.
712 (*B*) Overlap analysis of DEGs in *hac701* background with BTH-inducible and *OsWRKY45*-
713 dependent or *OsNPR1/NH1*-dependent genes (Table S8, S10). Significance values of the
714 overlap data were tested using the hypergeometric distribution test. (*C*) *OsWRKY45*-
715 dependent defense pathway components. (*D*) Gene expression of *OsWRKY45*-dependent
716 defense genes in 9-WT and *hac701*.

717

718 **Figure 4** Genome-wide H3K9 acetylation is depleted in *hac701*. (*A*) Heatmap showing the
719 accumulation of H3K9 acetylation on 265 peaks by taking the enrichment ratio of 9-WT and
720 *9-12b*$^{-/-}$ data (Wild type/mutant) (Table S15). (*B*) Heatmaps showing the accumulation of
721 H3K27 acetylation, H3K9 di-methylation, and H3K9 tri-methylation on 265 peaks by taking

722 the same enrichment ratio as (*A*). Heatmaps in (*A*) and (*B*) are representatives of two
723 biologically independent data showing similar enrichment results and number of peaks
724 identified. (*C*) GO enrichment analysis showing only the "Biological Process" of the 263 genes
725 found in the 265 peaks (Table S15). Numbers in enrichment indicate Fold Enrichment Value
726 using Fisher's Exact test with results for uncorrected $P<0.05$. (*D*) Enrichment scores of seven
727 representative genes showing depletion of H3K9 acetylation in *hac701*, *9-12b*$^{-/-}$. (*E*)
728 Enrichment scores of 10 representative putative decoy/sensor genes (42) showing depletion of
729 H3K9 acetylation in *hac701*, *9-12b*$^{-/-}$. Scores in (*D*) and (*E*) are averages of two biologically
730 independent ChIP-seq replicates with bars showing standard deviation (SD).

731

732 **Figure 5** *OsWRKY45* loci is enriched in H3K9 acetylation in *hac701*. (*A*) Enriched peaks on
733 histone modifications positioned to genomic locations (Intergenic, Promoter-TSS, Exon,
734 Intron, and TTS) in 9-WT and *hac701*, *9-12b*$^{-/-}$. All data were normalized to input. (*B*)
735 *OsWRKY45* depth graph of RNA-seq and H3K9 acetylation ChIP-seq showing the number of
736 reads in RPKM (Reads Per Kilobase of transcript, per Million mapped reads) in 9-WT and
737 *hac701*, *9-12b*$^{-/-}$. The red dotted box shows the 1kb upstream region of *OsWRKY45* with arrow
738 indicating the direction of transcription. (*C*) Upper panel: Gene map of *OsWRKY45* with arrow
739 showing the direction of transcription, gray bars are 5' and 3' untranslated regions (UTRs),
740 black bars are exons, and white bars are introns. Lower panel: 9-WT and *hac701* (*9-12b*$^{-/-}$)
741 mutant ChIP-qPCR showing enrichments of H3K9 acetylation and H3K9 di-methylation in
742 *OsWRKY45* locus. The significant difference in enrichment is computed using two-tailed
743 Student's *t*-test where asterisks: ***$P<0.01$, **$P<0.05$, and NS means Not Significant.

744

745

TABLE LEGENDS

None

SUPPLEMENTARY FIGURE LEGENDS

Figure S1 Characterization of mutations generated by CRISPR/Cas9 editing on the first and fifth exon of rice acetyltransferase gene, *HAC701*. (*A*) Schematic showing an sgRNA targeted to the first exon of *HAC701* gene. (*B*) PCR and RFLP assays of representative T0 and T1 generation lines from leaf blade (Lb), panicle (Pa), and seed (S) DNA samples. +/+ and M represent the zygosity of the line, where +/+ refers to wild type and M refers to monoallelic. (*C*) Alleles from 12 T0 generation lines identified by cloning and sequencing the PCR products from *HAC701* target regions using the primers found in Table S1. Similar line number indicates that lines came from the same callus. For each line, four DNA amplicons were cloned and sequenced and the fraction indicates the number of times the type of mutations were found in each line. In case not indicated, it means wild type. The asterisk (*) indicates the most common mutation found within and across different lines. (*D*) Upper panel: Schematic showing an sgRNA targeted to the fifth exon of *HAC701*. Lower panel: Schematic showing the protein domains of HAC701. (*E*) PCR and RFLP assays of representative T0 and T1 generation lines from leaf blade DNA samples. M, B represent the zygosity of the line, where M refers to monoallelic, and B refers to biallelic. T1 lines came from parental 2-3 line. (*F*) Phenotype of T2 lines showing effective grains and tiller number. (*G*) Images of T3 *hac701* lines compared to segregated wild type, 9-WT. (*H*) RT-qPCR levels of *HAC703* and *HAC704* genes in *HAC701* mutation line background. Samples were treated hydroponically with HDAC inhibitors (1µM Trichostatin A (TSA) and 100 µM Nicotinamide at final concentration) for three days. Bars represent standard error (SE); n= 3. The significant difference in transcription is computed using two-tailed Student's *t*-test where asterisks: *P<0.01. (*I*) Phenotype of T3 and T4 lines showing grain weight.

772 **Figure S2** flg22 induced the expression of rice pathogenesis-related and histone
773 acetyltransferase (HAT) gene, *HAC701*. Transcriptional levels of pathogenesis-related gene,
774 *PR10a*, and of eight HAT genes upon flg22 induction at concentrations in µM units. Data
775 shown are means ± SE; n= 3. The significant difference in transcription is computed using two-
776 tailed Student's *t*-test where asterisks: ***$P \leq 0.01$, **$P \leq 0.03$, * $P \leq 0.05$.

777

778 **Figure S3** *Pseudomonas syringae* pv. *oryzae* (*Pso*) infection assay in T2 *hac701* line, *9-12a*$^{-/-}$
779 . Values from 4th-6th serial dilutions were used for quantification. Segregated wild type line
780 was used as a control. Bars represent the 95% confidence interval (CI) and compared to wild
781 type using one-tailed Student's *t*-test at $P<0.05$.

782

783 **Figure S4** Sample distances of RNA-seq data after regularized-logarithm transformation
784 (rlog). Heatmap showing the Euclidean sample distance matrix of mock- and *Pseudomonas*
785 *syringae* pv. *oryzae* (*Pso*)-treated samples in two biologically independent replicates.

786

787 **Figure S5** Top 10 genes that are most highly variable in mock- and *Pso*-treated RNA-seq
788 samples. Gene descriptions were derived from Oryzabase: Integrated Rice Science Database
789 (NBRP) and Rice Genome Annotation Project (NSF). Two biologically independent RNA-seq
790 replicates are presented.

791

792 **Figure S6** Rice-*Pseudomonas syringae* pv. *oryzae* (*Pso*) pathosystem. (*A*) Enriched pathways
793 in the rice-*Pso* pathosystem. (*B*) Pie chart of the number of up- and down-regulated genes in
794 9-WT control 72h post *Pso* infection (Table S3). Two biologically independent RNA-seq data

795 in mock and *Pso* treatments are presented where differentially expressed genes (DEGs) were
796 selected at *P* adjusted value < 0.01.

797

798 **Figure S7** Features of differentially expressed genes (DEGs) in *Pseudomonas syringae* pv.
799 *oryzae* (*Pso*)-treated 9-WT and *hac701* transcriptomes. Overlap and GO-analysis of
800 upregulated (*A*) and downregulated (*B*) genes in *hac701* under *Pso* treatment (Table S3, S4).
801 Transcriptome data were normalized using mock data sets for each genotype. GO enrichment
802 analysis showing only the "Biological Process" of upregulated *HAC701*-repressed genes (141)
803 and HAC701-independent genes (336), downregulated *HAC701*-enhanced genes (31) and
804 HAC701-independent genes (46). Fold Enrichment Value uses Fisher's Exact test with results
805 for uncorrected $P<0.05$.

806

807 **Figure S8** Alignment of KIX domain found in different organisms. KIX domain in HAC701
808 (*A*) and HAC703 (*B*) proteins. Sc: *Saccharomyces cerevisiae*, Os: *Oryza sativa*, Hs: *Homo*
809 *sapiens*, Ce: *Caenorhabditis elegans*, Dm: *Drosophila melanogaster*, Mm: *Mus musculus*.

810

811 **Figure S9** *OsWRKY45* promoter contains a rare CRE motif. (*A*) A CRE motif (upper panel)
812 matches significantly to the query motif CGRCGRCG (lower panel). The query motif was
813 derived from discovered motifs (Table S13) in the 1 kb promoter regions of differentially
814 expressed genes (DEGs) in *hac701* treated with *Pso*. (*B*) 5 genes out of 660 differentially
815 expressed genes (DEGs) (0.76%) (Table S6) in the *hac701* contain the full CRE motif. Cister
816 parameter settings: default settings were used. *(C)* CRE motif cluster found in 1kb upstream
817 sequences of *OsWRKY45* start site. The red line indicates the probability of transcription factors
818 binding to these CRE motif sites. CRE motif is found most probably on the direct strand (+).

819 **Figure S10** Enrichment strength of ChIP signals in 9-WT input and histone modifications.

820

821 **Figure S11** Heatmaps of genome-wide histone modification enrichments in genes and
822 transposable elements (TEs) of rice 9-WT and *hac701* (*9-12b*$^{-/-}$) mutant. Enrichment of H3K9
823 acetylation, H3K9 di-methylation, H3K9 tri-methylation, H3K27 acetylation, and H3 in genes
824 (*A*) and TE (*B*) regions. Data represent one of the two biologically independent samples
825 showing similar enrichment results.

826 **Figure S12** Heatmaps of genome-wide histone modification enrichments in simple repeats of
827 rice 9-WT and *hac701* (*9-12b*$^{-/-}$) mutant. Enrichment of H3K9 acetylation, H3K9 di-
828 methylation, H3K9 tri-methylation, H3K27 acetylation, and H3 in simple repeat regions. Data
829 represent one of the two biologically independent samples showing similar enrichment results.

830

831 **Figure S13** Enrichment scores of additional representative genes showing differential
832 enrichments of H3K9 acetylation in *hac701* (*9-12b*$^{-/-}$) mutant. (*A*) Transcriptional coactivator
833 genes showing reduced or partially reduced H3K9 acetylation enrichments. (*B*) Putative
834 guardee genes showing differential enrichments of H3K9 acetylation. Scores are averages of
835 two biologically independent ChIP-seq replicates with bars showing standard deviation (SD).

836

837 **Figure S14** Distribution on genomic locations of 265 regions in H3K9 acetylation ChIP (wild
838 type/mutant).

839

840 **Figure S15** *OsWRKY45* depth graph of H3K9 and H3K27 acetylation ChIP-seq showing the
841 number of reads in RPKM (Reads Per Kilobase of transcript, per Million mapped reads) in 9-

842 WT and *hac701* (*9-12b*$^{-/-}$) mutant. The red dotted box shows the 1 kb upstream region of
843 *OsWRKY45* with arrow indicating the direction of transcription. Data show a representative
844 sample.

845

846 **Figure S16** Systemic gene expression analysis in rice-*Pseudomonas syringae* pv. *oryzae* (*Pso*)
847 pathosystem. (*A*) Differentially expressed genes (DEGs) in the local (870) and systemic (24)
848 tissues of plants infected with *Pso* (Table S16). Eight DEGs were found to be common in both
849 local and systemic tissues. (*B*) The expression of eight DEGs shown in log2 fold changes. For
850 local tissue analysis, two independent RNA-seq samples in both treatments (mock and *Pso*)
851 are presented. For systemic tissue analysis, two independent RNA-seq samples in mock and
852 three in *Pso* treatment are presented. The number of reads are in RPKM (Reads Per Kilobase
853 of transcript, per Million mapped reads) in 9-WT and *hac701*.

854

855 **Figure S17** MA-plot of differentially expressed genes (DEGs) in systemic tissues of 9-WT and
856 *hac701* infected with *Pseudomonas syringae* pv. *oryzae* (*Pso*). (*A*) and (*B*) plots showing
857 differences in measurements of differentially expressed genes (DEGs). *P* adjusted value is set
858 at <0.01. For 9-WT and *hac701* samples, two independent RNA-seq samples in mock treatment
859 and three in *Pso* treatment are presented.

860

861 **Figure S18** *OsWRKY45*-dependent defense pathway is suppressed by *HAC701*. Defense-
862 related genes regulated directly and indirectly by *OsWRKY45* are negatively regulated by
863 *HAC701* resulting in resistance phenotype of *hac701* through *OsWRKY45* upregulation.

864

865

SUPPLEMENTARY TABLE LEGENDS

Table S1 sgRNA oligonucleotides used for CRISPR/Cas9 mutagenesis and primers for genotyping. Bold sequences in the guide RNAs are the Protospacer Adjacent Motif (PAM).

Table S2 Summary of total RNA-sequencing data in local tissues.

Table S3 Wild type (9-WT) differentially expressed genes (DEGs) in *Pso*.

Table S4 *HAC701* repressed and enhanced genes.

Table S5 *HAC701* mutation differentially expressed genes (DEGs) in Mock (*HAC701mut*-DEGs in Mock).

Table S6 *HAC701* mutation differentially expressed genes (DEGs) in *Pso* (*HAC701mut*-DEGs in *Pso*). The motifs were identified 1kb upstream sequence of the start codon.

Table S7 BTH-responsive genes (24 hpi) in microarray experiments (34, 35) (Shimono et al. 2007, The Plant Cell & Sugano et al. 2010, Plant Molecular Biology). Overlap genes were removed.

Table S8 BTH-inducible & WRKY45-dependent genes (33) (Nakayama et al. 2013, BMC Plant Biology).

889 **Table S9** Upregulated genes after DEX-induced *WRKY45* expression (33) (Nakayama et al.
890 2013, BMC Plant Biology).

891

892 **Table S10** BTH-inducible genes affected by rice *NPR1/NH1* knockdown (35) (Sugano et al.
893 2010, Plant Molecular Biology).

894

895 **Table S11** *HAC701* mutation differentially expressed genes (DEGs) found in BTH-WRKY45
896 regulated genes that contain W-box motifs. The motifs were identified 1 kb upstream sequence
897 of the start codon.

898 **Table S12** *HAC701* mutation differentially expressed genes (DEGs) found in BTH-WRKY45
899 and BTH-NPR1/NH1 regulated genes that contain W-box motifs. The motifs were identified
900 1 kb upstream sequence of the start codon.

901

902 **Table S13** Significantly enriched DNA motifs in HAC701 mutation differentially expressed
903 genes (DEGs) in *Pso* (HAC701mut-DEGs in *Pso*).

904

905 **Table S14** Rice ChIP-sequencing information of histone modifications.

906

907 **Table S15** Identified peaks in H3K9ac and their corresponding genes in 9-WT/*9-12b*$^{-/-}$ (wild
908 type/mutant). Colored boxes indicate the repeated genes.

909

910 **Table S16** Summary of total RNA-sequencing data in systemic tissues.

911

912 **Table S17** List of R genes upregulated in *hac701* in *Pso*.

913

914 **Table S18** Identified peaks in H3K9me3 and their corresponding genes in *9-12b*$^{-/-}$/Input
915 (mutant/Input). Colored boxes indicate repeated genes.

916

917 **Table S19** Oligonucleotides used for RT-qPCRs (1) and ChIP-qPCRs (2).

918

919 **ACKNOWLEDGEMENTS**

920 We thank OIST SQC for RNA-seq and ChIP-seq analysis. This project benefited greatly from
921 the comments of Drs. Yusuke Saijo, Hirofumi Nakagami, Justin Walley, Yasuhiro Kadota, and
922 from the members of the Plant Epigenetics Unit (OIST) and Plant Immunity Research Group
923 (RIKEN CSRS).

924

925 **FUNDING**

926 This work was supported in part by the Okinawa Institute of Science and Technology Graduate
927 University (OIST). N.A.E. was also funded by Grant-in-Aid for JSPS Fellows (Grant No:
928 18F18085). The funders had no role in study design, data collection and analysis, decision to
929 publish, or preparation of the manuscript.

930

931 **AUTHOR CONTRIBUTIONS**

932 NAE: Conceptualization, Data curation, Funding acquisition, Formal analysis, Investigation,
933 Visualization, Writing-original draft, Writing-review & editing

934 LNT: Data curation, Formal analysis, Writing-review & editing

935 SM: Formal analysis, Investigation

YS: Formal analysis, Investigation

KS: Funding acquisition, Formal analysis, Supervision, Writing-review & editing

HS: Funding acquisition, Formal analysis, Investigation, Supervision, Writing-review & editing

COMPETING INTERESTS

The authors have declared that no competing interests exist.

REFERENCES

1. Lee KK & Workman JL (2007) Histone acetyltransferase complexes: one size doesn't fit all. *Nat. Rev. Mol. Cell Biol.* 8(4):284-295.

2. Chan HM & La Thangue NB (2001) p300/CBP proteins: HATs for transcriptional bridges and scaffolds. *J. Cell Sci.* 114(Pt 13):2363-2373.

3. Kalkhoven E (2004) CBP and p300: HATs for different occasions. *Biochem. Pharmacol.* 68(6):1145-1155.

4. Janknecht R & Hunter T (1996) Transcription. A growing coactivator network. *Nature* 383(6595):22-23.

5. Goodrich JA & Tjian R (1994) TBP-TAF complexes: selectivity factors for eukaryotic transcription. *Curr. Opin. Cell Biol.* 6(3):403-409.

6. Pandey R*, et al.* (2002) Analysis of histone acetyltransferase and histone deacetylase families of Arabidopsis thaliana suggests functional diversification of chromatin modification among multicellular eukaryotes. *Nucleic Acids Res.* 30(23):5036-5055.

7. Liu X*, et al.* (2012) Histone acetyltransferases in rice (Oryza sativa L.): phylogenetic analysis, subcellular localization and expression. *BMC Plant Biol.* 12:145.

8. Fang H, Liu X, Thorn G, Duan J, & Tian L (2014) Expression analysis of histone acetyltransferases in rice under drought stress. *Biochem. Biophys. Res. Commun.* 443(2):400-405.

9. Ma X, Lv S, Zhang C, & Yang C (2013) Histone deacetylases and their functions in plants. *Plant Cell Rep.* 32(4):465-478.

10. Song G & Walley JW (2016) Dynamic Protein Acetylation in Plant–Pathogen Interactions. *Frontiers in plant science* 7.

11. Ding B & Wang GL (2015) Chromatin versus pathogens: the function of epigenetics in plant immunity. *Frontiers in plant science* 6:675.

12. Zhu QH, Shan WX, Ayliffe MA, & Wang MB (2016) Epigenetic Mechanisms: An Emerging Player in Plant-Microbe Interactions. *Molecular plant-microbe interactions : MPMI* 29(3):187-196.

13. Fu W, Wu K, & Duan J (2007) Sequence and expression analysis of histone deacetylases in rice. *Biochem. Biophys. Res. Commun.* 356(4):843-850.

14. Yuan LW & Giordano A (2002) Acetyltransferase machinery conserved in p300/CBP-family proteins. *Oncogene* 21(14):2253-2260.

15. Ogryzko VV, Schiltz RL, Russanova V, Howard BH, & Nakatani Y (1996) The transcriptional coactivators p300 and CBP are histone acetyltransferases. *Cell* 87(5):953-959.

16. Bannister AJ & Kouzarides T (1996) The CBP co-activator is a histone acetyltransferase. *Nature* 384(6610):641-643.

17. Henry RA, Kuo YM, & Andrews AJ (2013) Differences in specificity and selectivity between CBP and p300 acetylation of histone H3 and H3/H4. *Biochemistry* 52(34):5746-5759.

18. Jin Q*, et al.* (2011) Distinct roles of GCN5/PCAF-mediated H3K9ac and CBP/p300-mediated H3K18/27ac in nuclear receptor transactivation. *EMBO J.* 30(2):249-262.

19. Tie F*, et al.* (2009) CBP-mediated acetylation of histone H3 lysine 27 antagonizes Drosophila Polycomb silencing. *Development* 136(18):3131-3141.

20. Das C, Lucia MS, Hansen KC, & Tyler JK (2009) CBP/p300-mediated acetylation of histone H3 on lysine 56. *Nature* 459(7243):113-117.

21. Schiltz RL*, et al.* (1999) Overlapping but distinct patterns of histone acetylation by the human coactivators p300 and PCAF within nucleosomal substrates. *J. Biol. Chem.* 274(3):1189-1192.

22. Sakamoto S*, et al.* (2012) E2A and CBP/p300 act in synergy to promote chromatin accessibility of the immunoglobulin kappa locus. *J. Immunol.* 188(11):5547-5560.

23. Modak R*, et al.* (2013) Probing p300/CBP associated factor (PCAF)-dependent pathways with a small molecule inhibitor. *ACS chemical biology* 8(6):1311-1323.

997 24. Espinas NA, Saze H, & Saijo Y (2016) Epigenetic Control of Defense Signaling and
998 Priming in Plants. *Frontiers in plant science* 7.

999 25. Kuwata H (1985) Pseudomonas syringiae pv. oryzae pv. nov., causal agent of
1000 bacterial halo blight of rice. *Ann Phytopath. Soc. Japan* 51:212-218.

1001 26. Kang S, Kang K, Lee K, & Back K (2007) Characterization of rice tryptophan
1002 decarboxylases and their direct involvement in serotonin biosynthesis in transgenic
1003 rice. *Planta* 227(1):263-272.

1004 27. Ishihara A*, et al.* (2008) The tryptophan pathway is involved in the defense responses
1005 of rice against pathogenic infection via serotonin production. *Plant J.* 54(3):481-495.

1006 28. Shimizu T*, et al.* (2012) Purification and identification of naringenin 7-O-
1007 methyltransferase, a key enzyme in biosynthesis of flavonoid phytoalexin sakuranetin
1008 in rice. *J. Biol. Chem.* 287(23):19315-19325.

1009 29. Ogawa S*, et al.* (2017) OsMYC2, an essential factor for JA-inductive sakuranetin
1010 production in rice, interacts with MYC2-like proteins that enhance its transactivation
1011 ability. *Scientific reports* 7:40175.

1012 30. Swaminathan S, Morrone D, Wang Q, Fulton DB, & Peters RJ (2009) CYP76M7 is
1013 an ent-cassadiene C11alpha-hydroxylase defining a second multifunctional
1014 diterpenoid biosynthetic gene cluster in rice. *Plant Cell* 21(10):3315-3325.

1015 31. Vanholme R, Demedts B, Morreel K, Ralph J, & Boerjan W (2010) Lignin
1016 biosynthesis and structure. *Plant Physiol.* 153(3):895-905.

1017 32. Wang Q*, et al.* (2012) Characterization of CYP76M5-8 indicates metabolic plasticity
1018 within a plant biosynthetic gene cluster. *J. Biol. Chem.* 287(9):6159-6168.

1019 33. Nakayama A*, et al.* (2013) Genome-wide identification of WRKY45-regulated genes
1020 that mediate benzothiadiazole-induced defense responses in rice. *BMC Plant Biol.*
1021 13(150).

1022 34. Shimono M*, et al.* (2007) Rice WRKY45 plays a crucial role in benzothiadiazole-
1023 inducible blast resistance. *Plant Cell* 19(6):2064-2076.

1024 35. Sugano S*, et al.* (2010) Role of OsNPR1 in rice defense program as revealed by
1025 genome-wide expression analysis. *Plant Mol. Biol.* 74(6):549-562.

1026 36. Cheng X*, et al.* (2019) Structural basis of dimerization and dual W-box DNA
1027 recognition by rice WRKY domain. *Nucleic Acids Res.* 47(8):4308-4318.

37. Parker D, *et al.* (1996) Phosphorylation of CREB at Ser-133 induces complex formation with CREB-binding protein via a direct mechanism.pdf>. *Mol. Cell. Biol.*:694-703.

38. Yadav A, Thakur JK, & Yadav G (2017) KIXBASE: A comprehensive web resource for identification and exploration of KIX domains. *Scientific reports* 7(1):14924.

39. Thakur JK, Yadav A, & Yadav G (2014) Molecular recognition by the KIX domain and its role in gene regulation. *Nucleic Acids Res.* 42(4):2112-2125.

40. Dancy BM & Cole PA (2015) Protein Lysine Acetylation by p300/CBP. *Chemical reviews* 115(6):2419-2452.

41. Du Z, *et al.* (2013) Genome-wide analysis of histone modifications: H3K4me2, H3K4me3, H3K9ac, and H3K27ac in Oryza sativa L. Japonica. *Molecular plant* 6(5):1463-1472.

42. Sarris PF, Cevik V, Dagdas G, Jones JD, & Krasileva KV (2016) Comparative analysis of plant immune receptor architectures uncovers host proteins likely targeted by pathogens. *BMC Biol.* 14:8.

43. Weidenbach D, *et al.* (2016) Polarized Defense Against Fungal Pathogens Is Mediated by the Jacalin-Related Lectin Domain of Modular Poaceae-Specific Proteins. *Molecular plant* 9(4):514-527.

44. Chen X, *et al.* (2019) Transcriptome and Proteome Profiling of Different Colored Rice Reveals Physiological Dynamics Involved in the Flavonoid Pathway. *International journal of molecular sciences* 20(10).

45. Holler S, *et al.* (2015) Ascorbate biosynthesis and its involvement in stress tolerance and plant development in rice (Oryza sativa L.). *Plant Mol. Biol.* 88(6):545-560.

46. Singh P, *et al.* (2014) Environmental History Modulates Arabidopsis Pattern-Triggered Immunity in a HISTONE ACETYLTRANSFERASE1-Dependent Manner. *Plant Cell*.

47. Kim S, *et al.* (2020) GCN5 modulates salicylic acid homeostasis by regulating H3K14ac levels at the 5' and 3' ends of its target genes. *Nucleic Acids Res.* 48(11):5953-5966.

48. De Vleesschauwer D, Gheysen G, & Hofte M (2013) Hormone defense networking in rice: tales from a different world. *Trends Plant Sci.* 18(10):555-565.

49. Vidhyasekaran P (2016) *Switching on plant innate immunity signaling systems* (Springer International Publishing, Switzerland).

50. De Vleesschauwer D, Xu J, & Hofte M (2014) Making sense of hormone-mediated defense networking: from rice to Arabidopsis. *Frontiers in plant science* 5:611.

51. Yang DL, Yang Y, & He Z (2013) Roles of plant hormones and their interplay in rice immunity. *Molecular plant* 6(3):675-685.

52. Yan S & Dong X (2014) Perception of the plant immune signal salicylic acid. *Curr. Opin. Plant Biol.* 20:64-68.

53. Silverman P*, et al.* (1995) Salicylic acid in rice (biosynthesis, conjugation, and possible role). *Plant Physiol.* 108:633-639.

54. Chen Z, Iyer S, Caplan A, Klessig DF, & Fan B (1997) Differential accumulation of salicylic acid and salicylic acid-sensitive catalase in different rice tissues. *Plant Physiol.* 114:193-201.

55. Hiebert CW*, et al.* (2020) Stem rust resistance in wheat is suppressed by a subunit of the mediator complex. *Nature communications* 11(1):1123.

56. Brownell JE & Allis CD (1996) Special HATs for special occasions: linking histone acetylation to chromatin assembly and gene activation. *Curr. Opin. Genet. Dev.* 6:176-184.

57. Poss ZC, Ebmeier CC, & Taatjes DJ (2013) The Mediator complex and transcription regulation. *Crit. Rev. Biochem. Mol. Biol.* 48(6):575-608.

58. Canet JV, Dobon A, & Tornero P (2012) Non-recognition-of-BTH4, an Arabidopsis mediator subunit homolog, is necessary for development and response to salicylic acid. *Plant Cell* 24(10):4220-4235.

59. van der Hoorn RA & Kamoun S (2008) From Guard to Decoy: a new model for perception of plant pathogen effectors. *Plant Cell* 20(8):2009-2017.

60. Lai Y*, et al.* (2020) The Arabidopsis PHD-finger protein EDM2 has multiple roles in balancing NLR immune receptor gene expression. *PLoS Genet.* 16(9):e1008993.

61. Jackson JP*, et al.* (2004) Dimethylation of histone H3 lysine 9 is a critical mark for DNA methylation and gene silencing in Arabidopsis thaliana. *Chromosoma* 112(6):308-315.

62. Karasov T, Chae E, Herman J, & Bergelson J (2017) Mechanisms to Mitigate the Tradeoff between Growth and Defense. *Plant Cell*.

63. Huot B, Yao J, Montgomery BL, & He SY (2014) Growth-defense tradeoffs in plants: a balancing act to optimize fitness. *Molecular plant* 7(8):1267-1287.

64. Xie K & Yang Y (2013) RNA-guided genome editing in plants using a CRISPR-Cas system. *Molecular plant* 6(6):1975-1983.

65. Heese A*, et al.* (2007) The receptor-like kinase SERK3/BAK1 is a central regulator of innate immunity in plants. *Proceedings of the National Academy of Sciences of the United States of America* 104(29):12217-12222.

66. Park CJ & Ronald PC (2012) Cleavage and nuclear localization of the rice XA21 immune receptor. *Nature communications* 3:920.

67. Liu X*, et al.* (2015) Bacterial Leaf Infiltration Assay for Fine Characterization of Plant Defense Responses using the Arabidopsis thaliana-Pseudomonas syringae Pathosystem. *J Vis Exp* (104).

68. Pfaffl MW (2001) A new mathematical model for relative quantification in real-time RT-PCR. *Nucleic Acids Res.* 29(9):e45.

69. Saleh A, Alvarez-Venegas R, & Avramova Z (2008) An efficient chromatin immunoprecipitation (ChIP) protocol for studying histone modifications in Arabidopsis plants. *Nature protocols* 3(6):1018-1025.

70. Trapnell C, Pachter L, & Salzberg SL (2009) TopHat: discovering splice junctions with RNA-Seq. *Bioinformatics* 25(9):1105-1111.

71. Trapnell C*, et al.* (2012) Differential gene and transcript expression analysis of RNA-seq experiments with TopHat and Cufflinks. *Nature protocols* 7(3):562-578.

72. Love MI, Huber W, & Anders S (2014) Moderated estimation of fold change and dispersion for RNA-seq data with DESeq2. *Genome biology* 15(12):550.

73. Li Q, Brown JB, Huang H, & Bickel PJ (2011) Measuring reproducibility of high-throughput experiments. *The Annals of Applied Statistics* 5(3):1752-1779.

74. Consortium TGO (2017) Expansion of the Gene Ontology knowledgebase and resources. *Nucleic Acids Res.* 45(D1):D331-D338.

75. Consortium TGO (2000) Gene Ontology: tool for the unification of biology. *Nat. Genet.* 25:25-29.

76. Consortium TGO (2015) Gene Ontology Consortium: going forward. *Nucleic Acids Res.* 43(Database issue):D1049-1056.

77. Heberle H, Meirelles GV, da Silva FR, Telles GP, & Minghim R (2015) InteractiVenn: a web-based tool for the analysis of sets through Venn diagrams. *BMC Bioinformatics* 16:169.

78. Langmead B, Trapnell C, Pop M, & Salzberg SL (2009) Ultrafast and memory-efficient alignment of short DNA sequences to the human genome. *Genome biology* 10(3):R25.

79. Freese NH, Norris DC, & Loraine AE (2016) Integrated genome browser: visual analytics platform for genomics. *Bioinformatics* 32(14):2089-2095.

80. Ramirez F*, et al.* (2016) deepTools2: a next generation web server for deep-sequencing data analysis. *Nucleic Acids Res.* 44(W1):W160-165.

81. Quinlan AR & Hall IM (2010) BEDTools: a flexible suite of utilities for comparing genomic features. *Bioinformatics* 26(6):841-842.

82. Heinz S*, et al.* (2010) Simple combinations of lineage-determining transcription factors prime cis-regulatory elements required for macrophage and B cell identities. *Mol. Cell* 38(4):576-589.

83. Dereeper A*, et al.* (2008) Phylogeny.fr: robust phylogenetic analysis for the non-specialist. *Nucleic Acids Res.* 36(Web Server issue):W465-469.

84. Edgar RC (2004) MUSCLE: multiple sequence alignment with high accuracy and high throughput. *Nucleic Acids Res.* 32(5):1792-1797.

85. Frith M, Hansen U, & Weng Z (2001) Detection of cis-element clusters in higher eukaryotic DNA. *Bioinformatics* 17:878-889.

86. Bailey TL (2011) DREME: motif discovery in transcription factor ChIP-seq data. *Bioinformatics* 27(12):1653-1659.

Figure 1

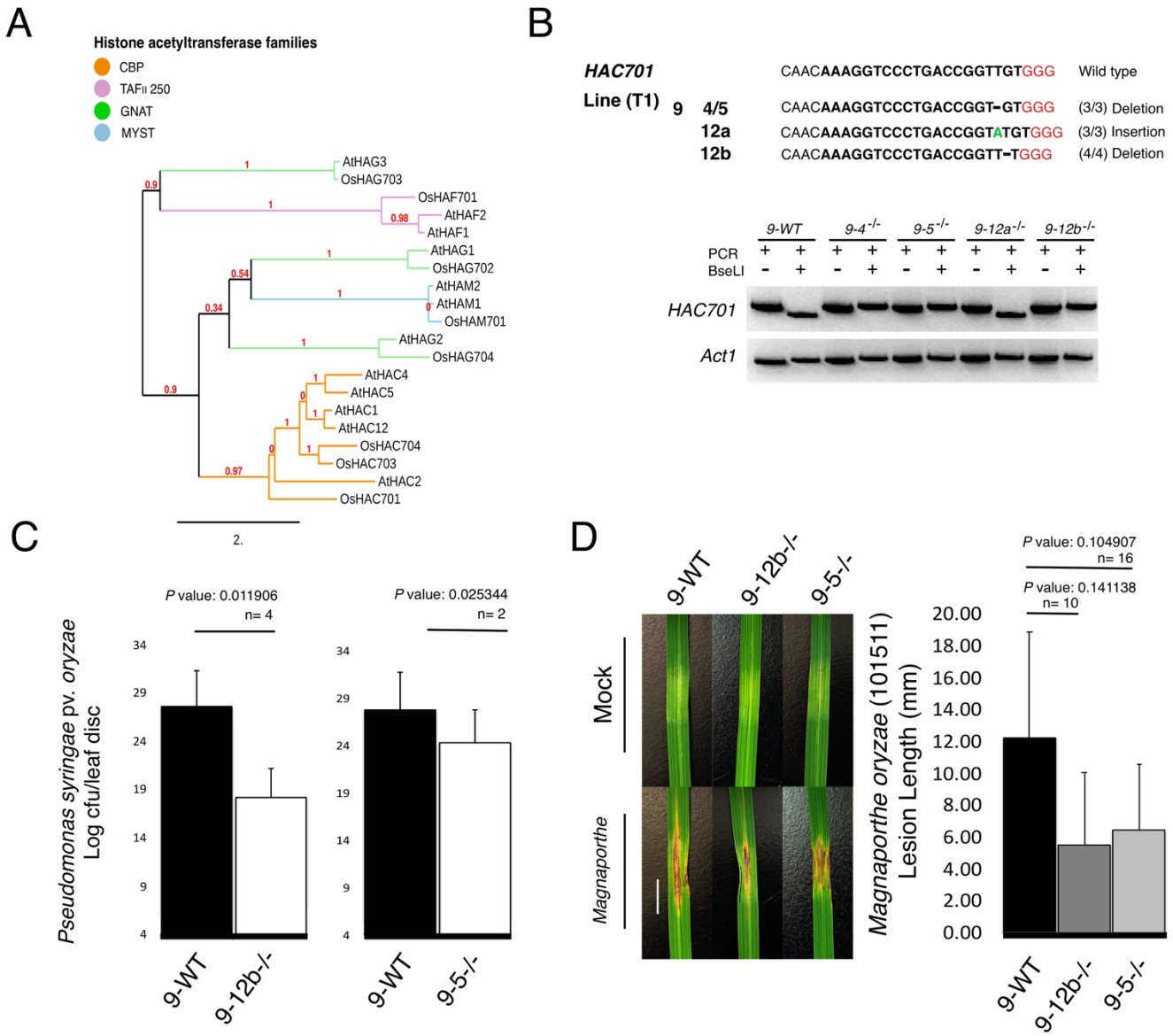

Figure 2

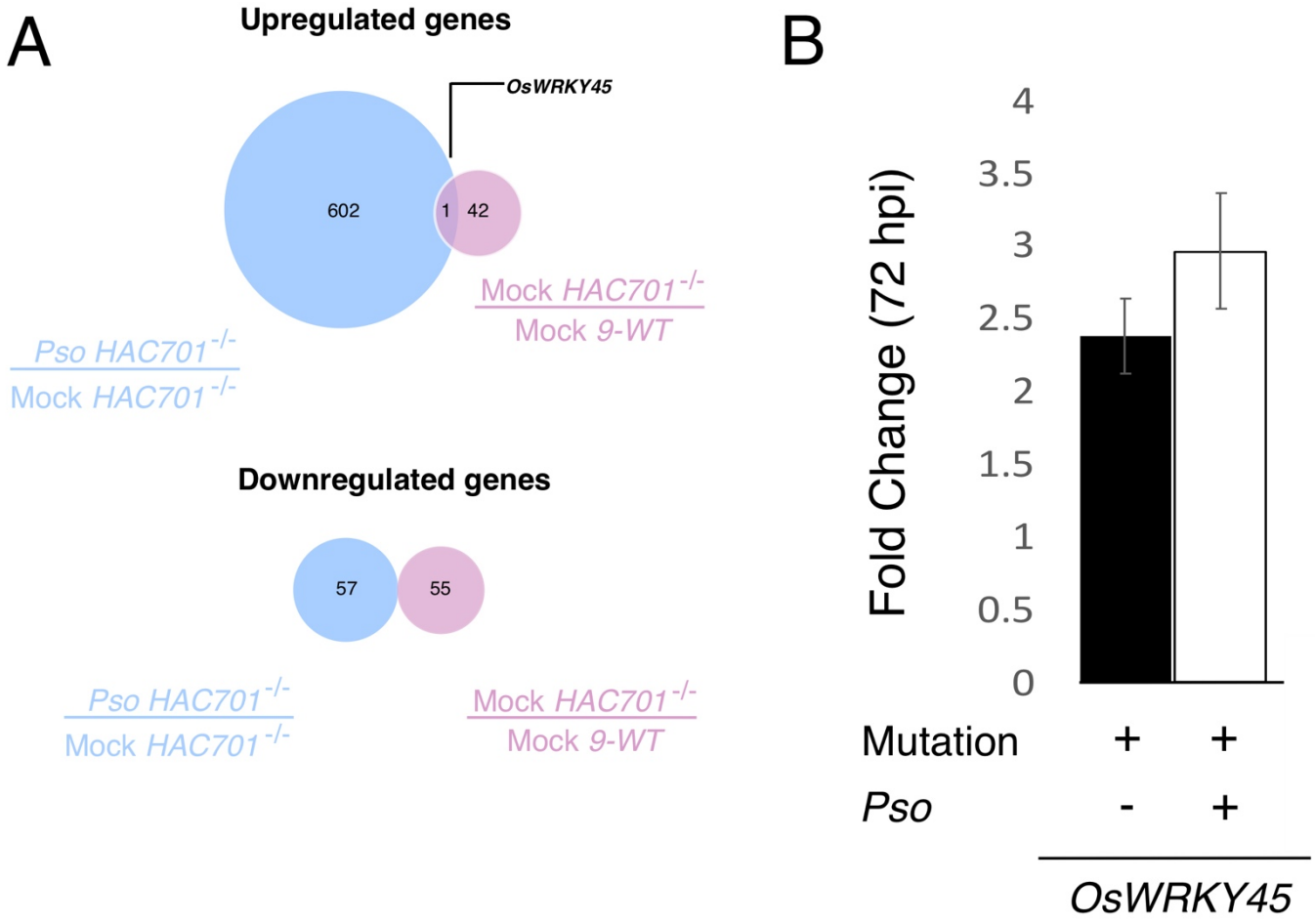

Figure 3

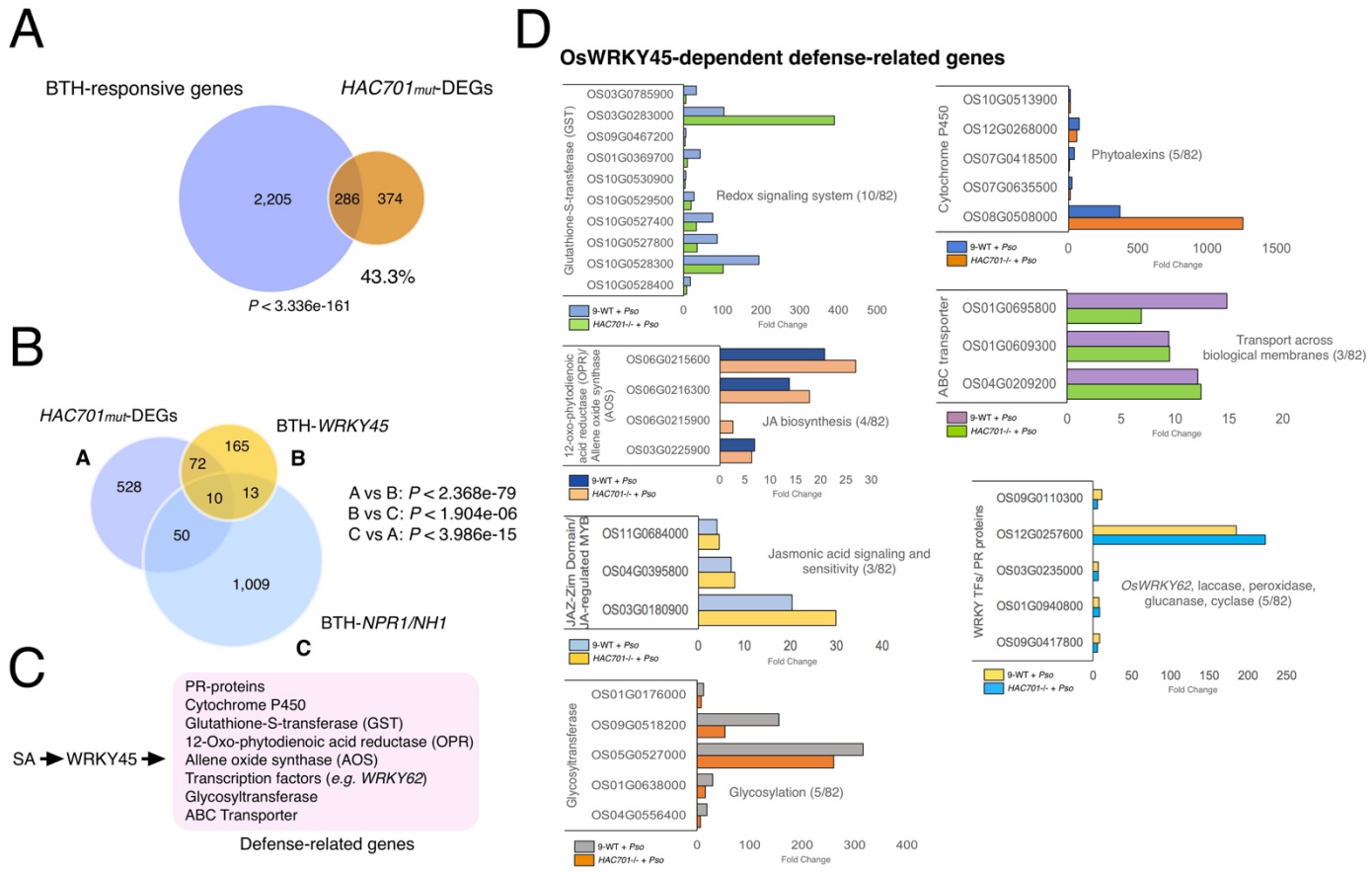

Figure 4

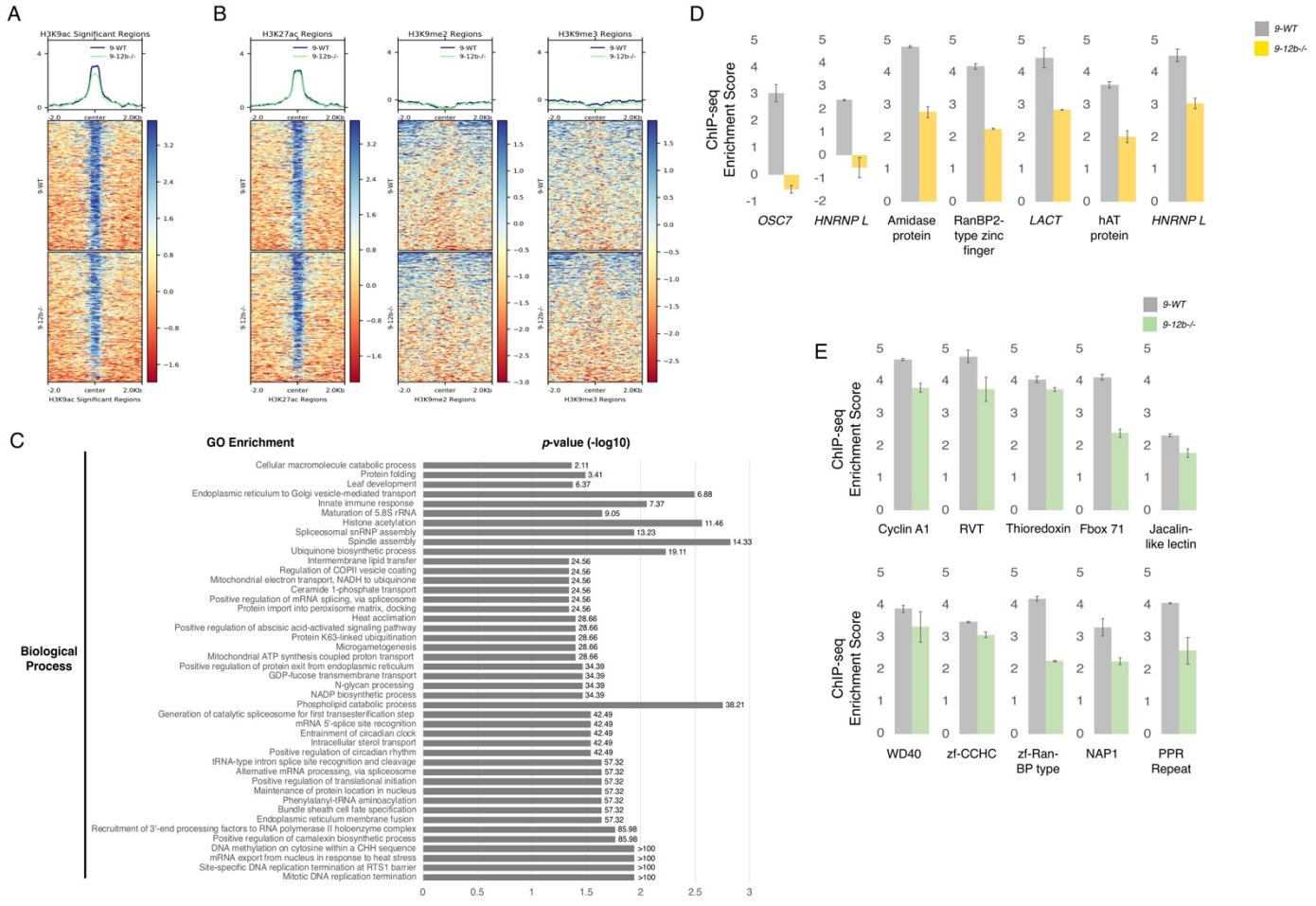

Figure 5

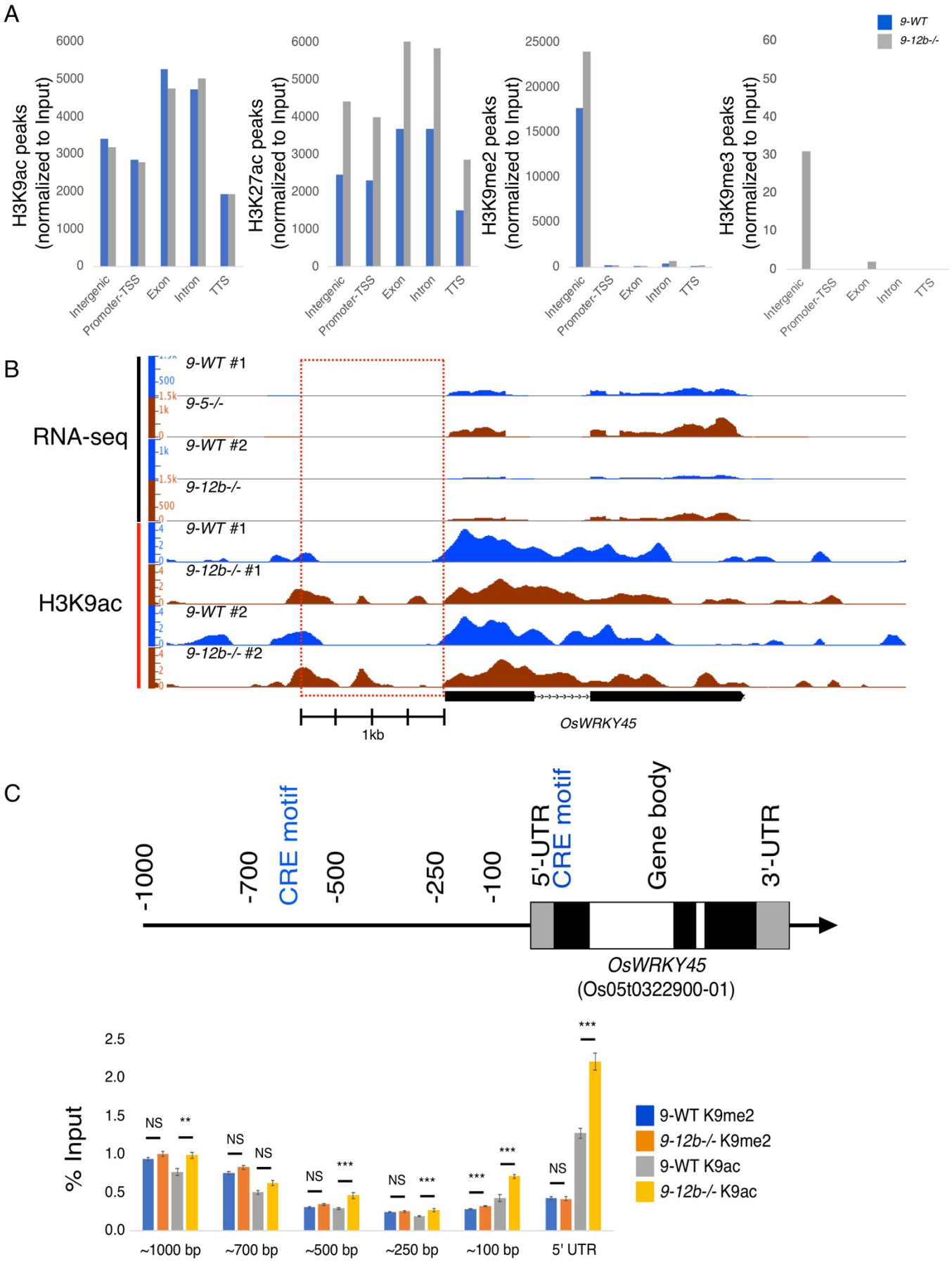

Figure S1

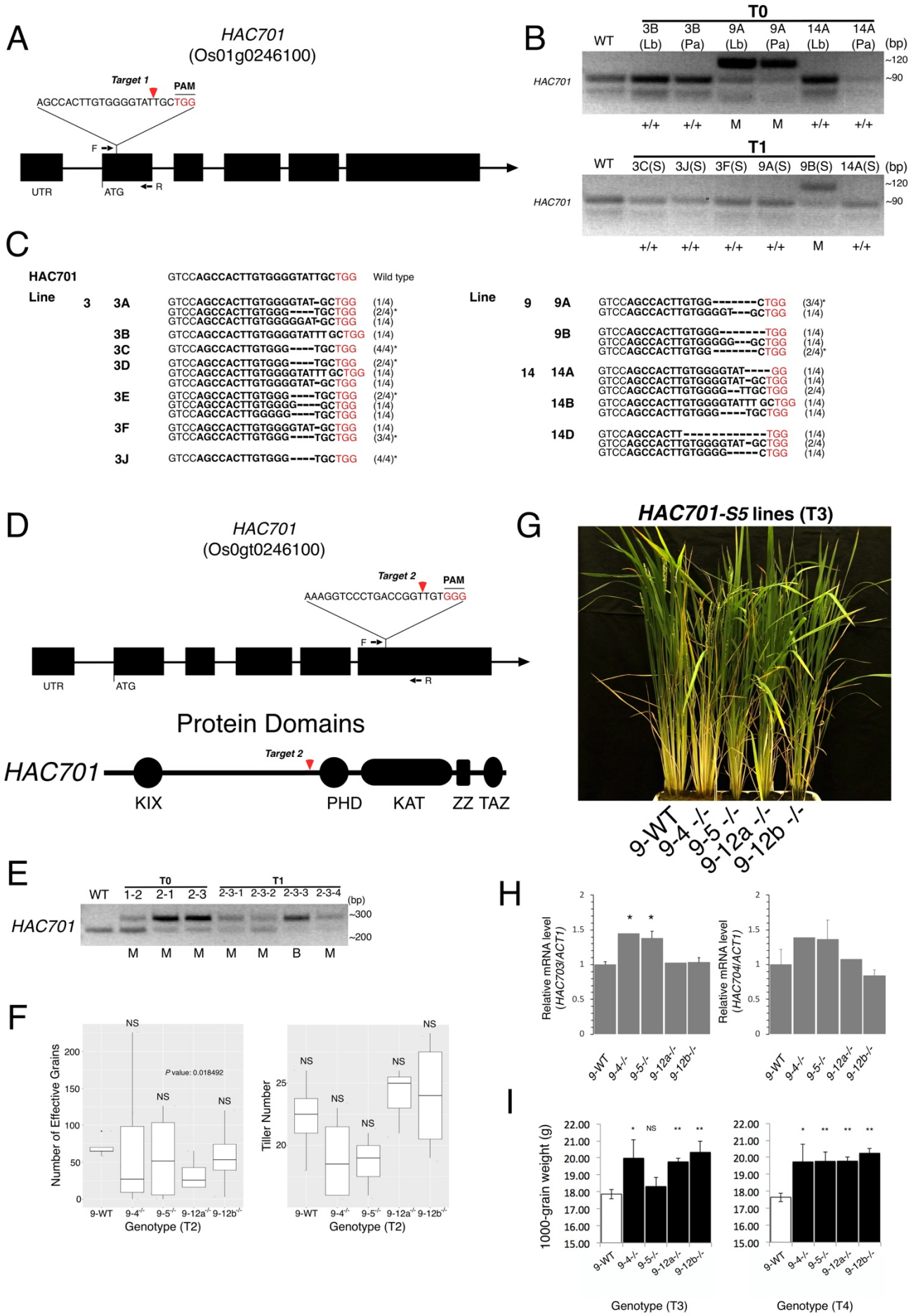

Figure S2

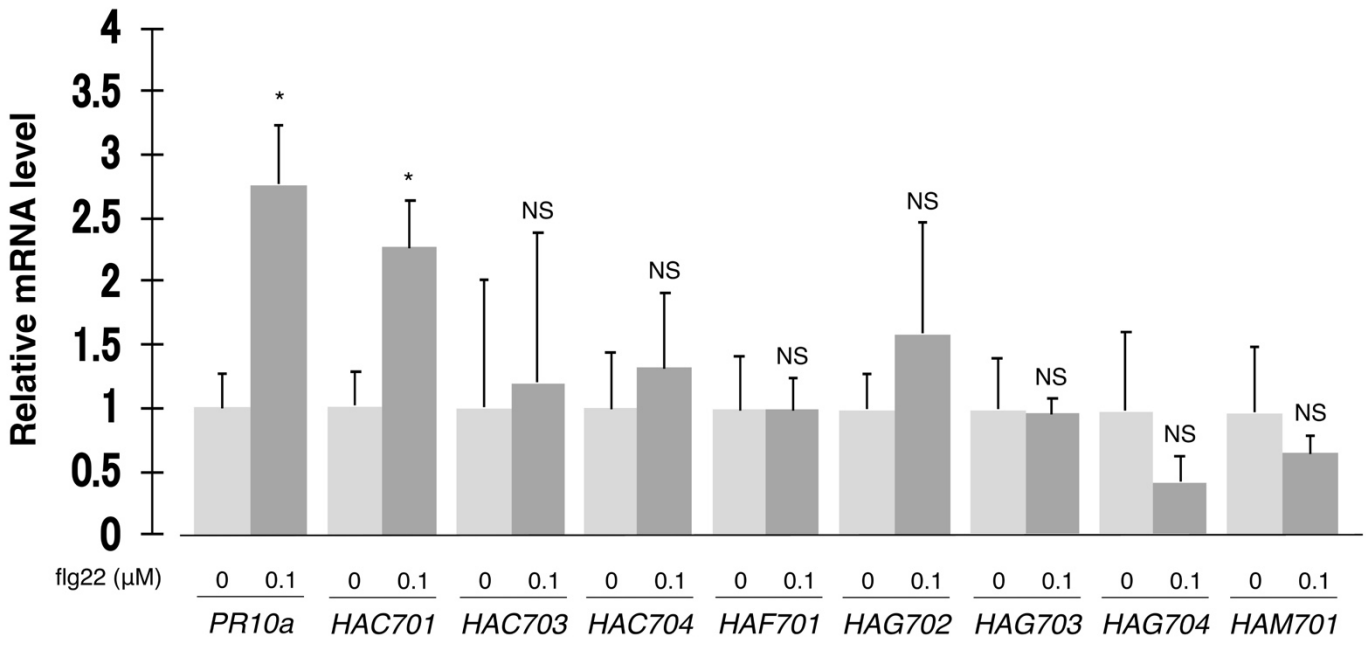

Figure S3

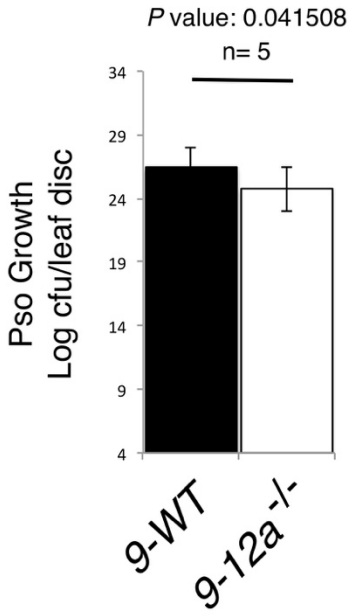

Figure S4

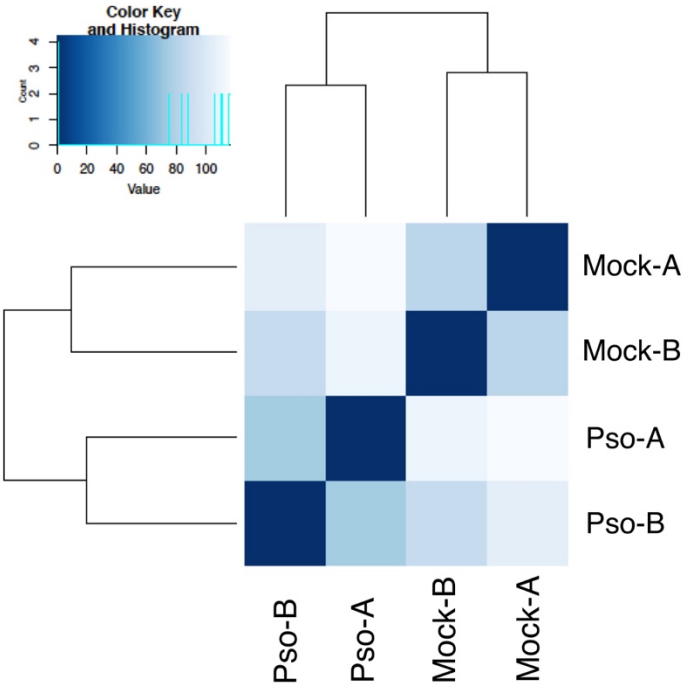

Figure S5

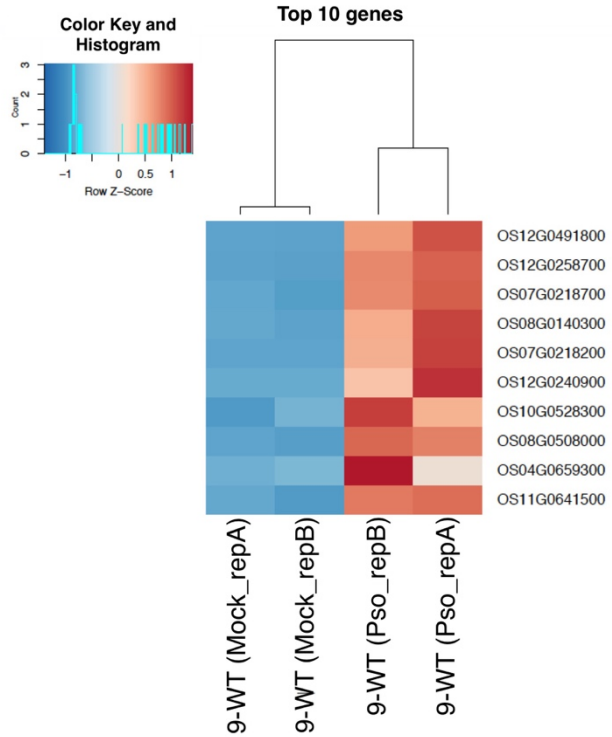

Gene ID	Description
OS12G0491800	Kaurene synthase-like 10
OS12G0258700	Laccase 29
OS07G0218700	Cytochrome P450 family protein
OS08G0140300	Tryptophan decarboxylase 1
OS07G0218200	Terpene synthase 3
OS12G0240900	Naringenin 7-O-methyltransferase
OS10G0528300	Tau glutathione S-transferase 4
OS08G0508000	Cytochrome P450 76M2
OS04G0659300	Root meander curling
OS11G0641500	Laccase 23

Figure S6

A

Highly enriched terms upon *Pseudomonas syringiae pv. oryzae* infection in 9-WT rice

Up-regulated terms	Fold Enrichment	raw P-value
Cell wall macromolecule catabolic process	54.94	4.22E-07
Adventitious root development	54.94	3.54E-02
Lignin biosynthetic process	54.94	3.54E-02
Sphingolipid biosynthetic process	54.94	3.54E-02
Gibberellin biosynthetic process	54.94	3.54E-02
Chitin catabolic process	54.94	4.22E-07
Response to wounding	54.94	3.54E-02
Response to other organism	54.94	2.70E-08
ent-kaurene oxidation to kaurenoic acid	54.94	3.54E-02
Diterpene phytoalexin precursor biosynthetic process pathway	41.21	1.89E-04
Shikimate biosynthetic process	36.63	3.08E-03
Chorismate biosynthetic process	36.63	3.08E-03
Carbohydrate transport	18.31	8.32E-03
Carbohydrate metabolic process	5.78	6.62E-03
Electron transport chain	5.49	1.17E-03
Regulation of transcription, DNA templated	2.79	2.43E-02

Down-regulated terms	Fold Enrichment	raw P-value
Regulation of transcription, DNA templated	10.26	1.69E-02

B

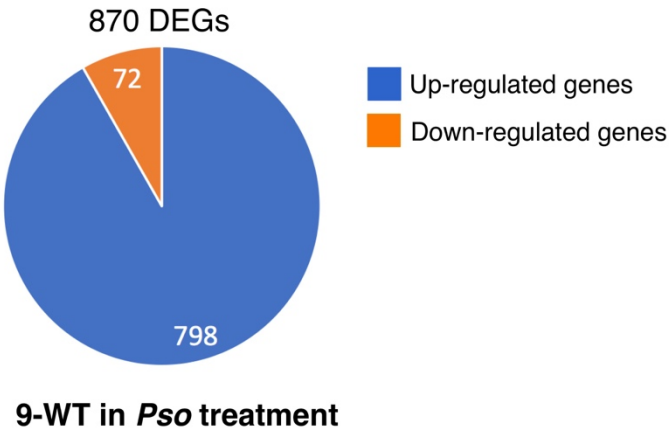

Figure S7

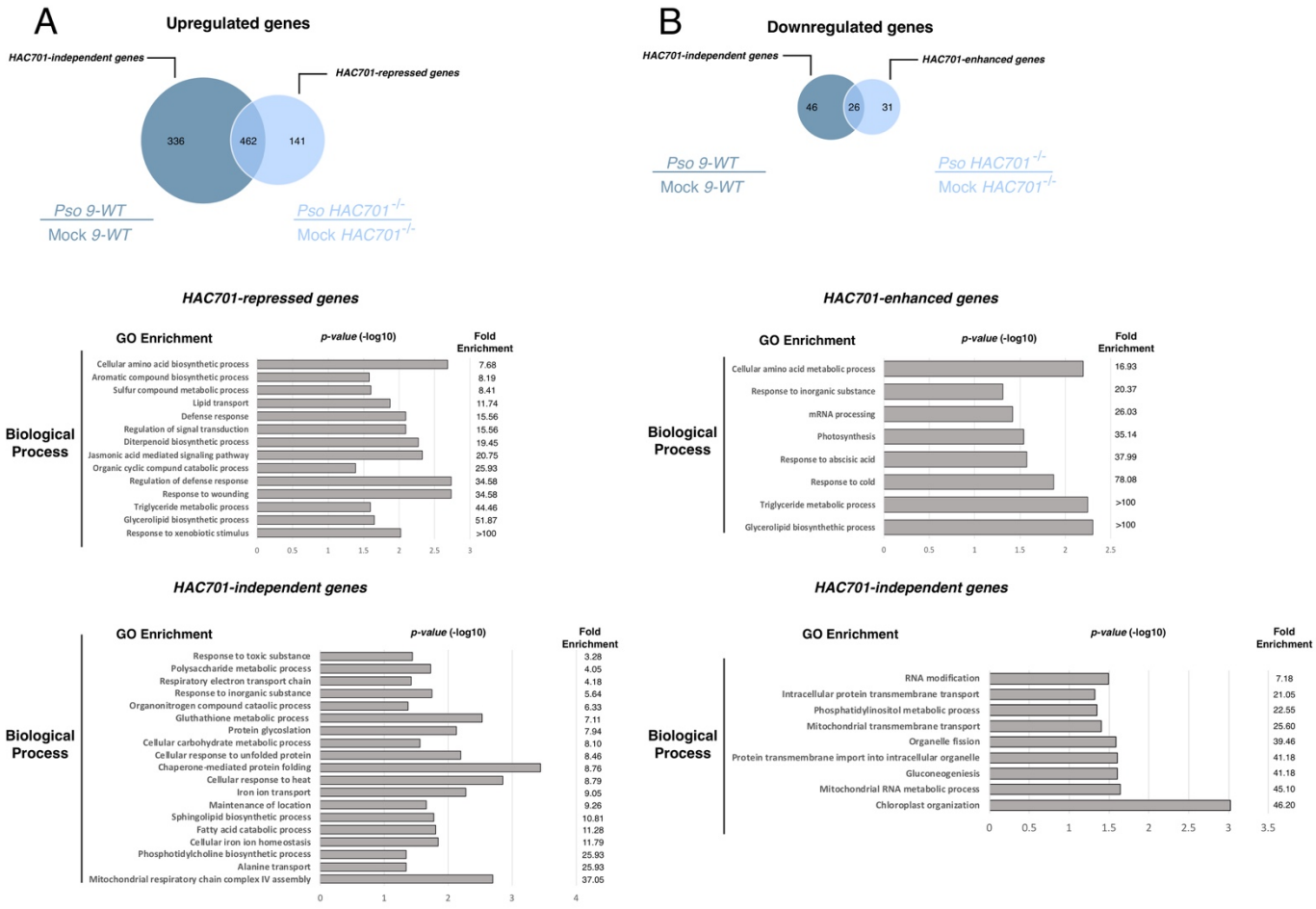

Figure S8

A

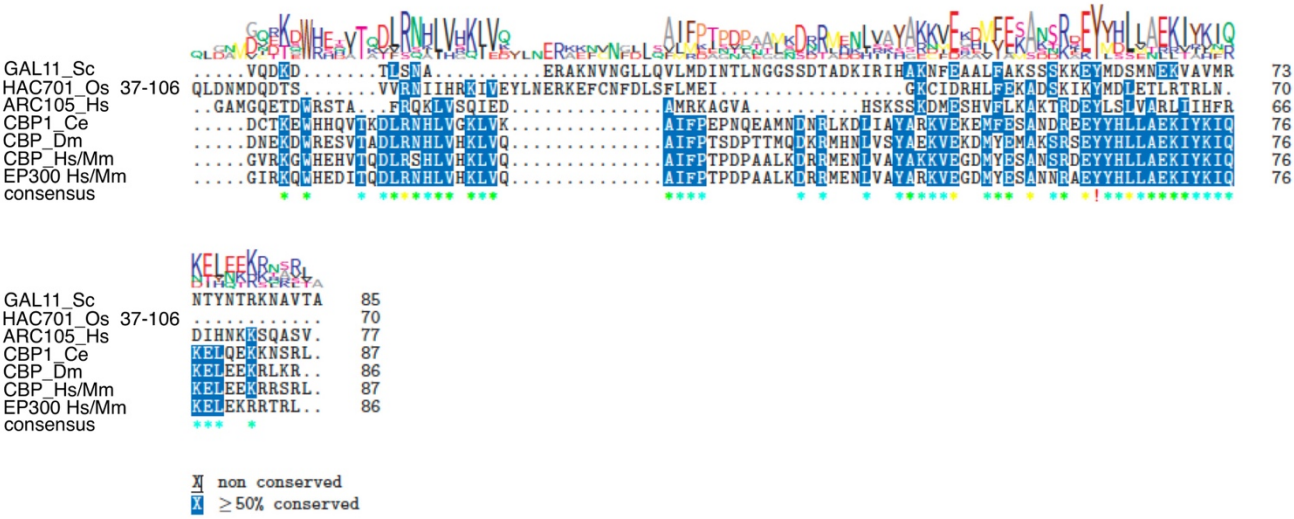

B

Figure S9

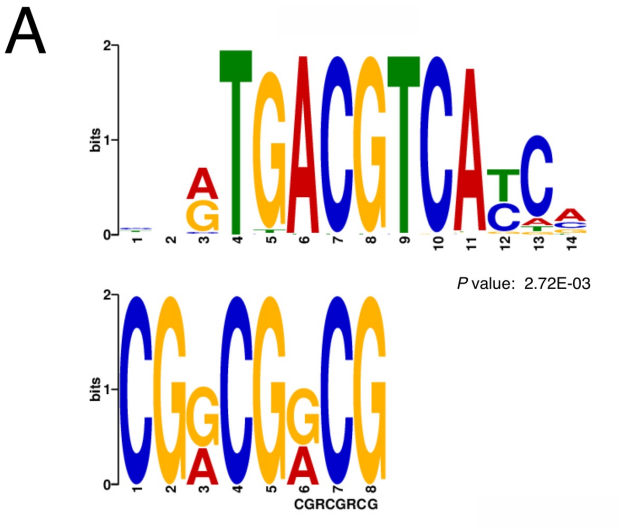

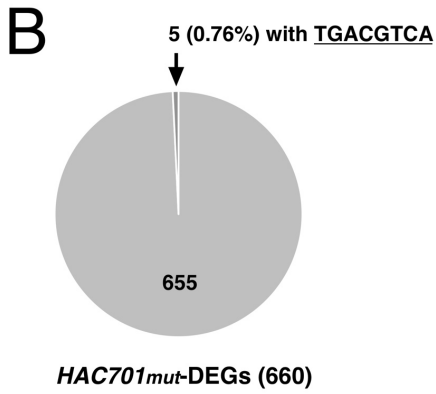

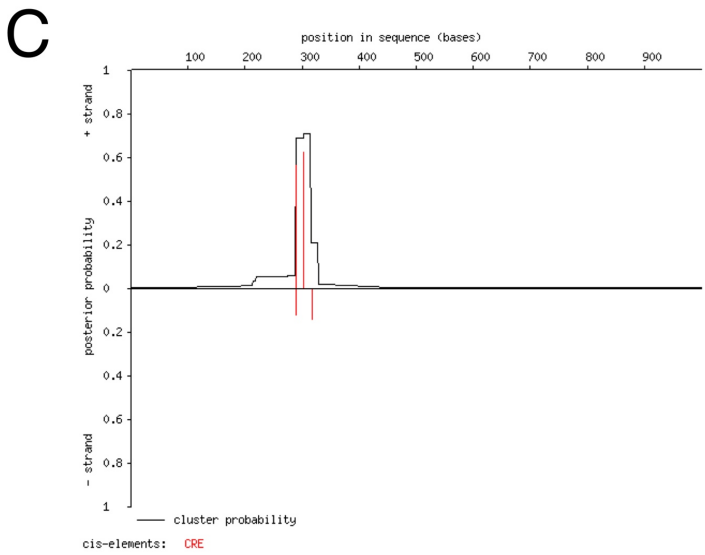

Possible functional cis-elements

Type	Position	Strand	Sequence	Probability
CRE	303-314	+	cgtgacgtcatc	0.62
CRE	289-300	+	gctgacgtcgcc	0.56
CRE	317-328	-	gttgtcgtcccc	0.14
CRE	289-300	-	gctgacgtcgcc	0.12

Figure S10

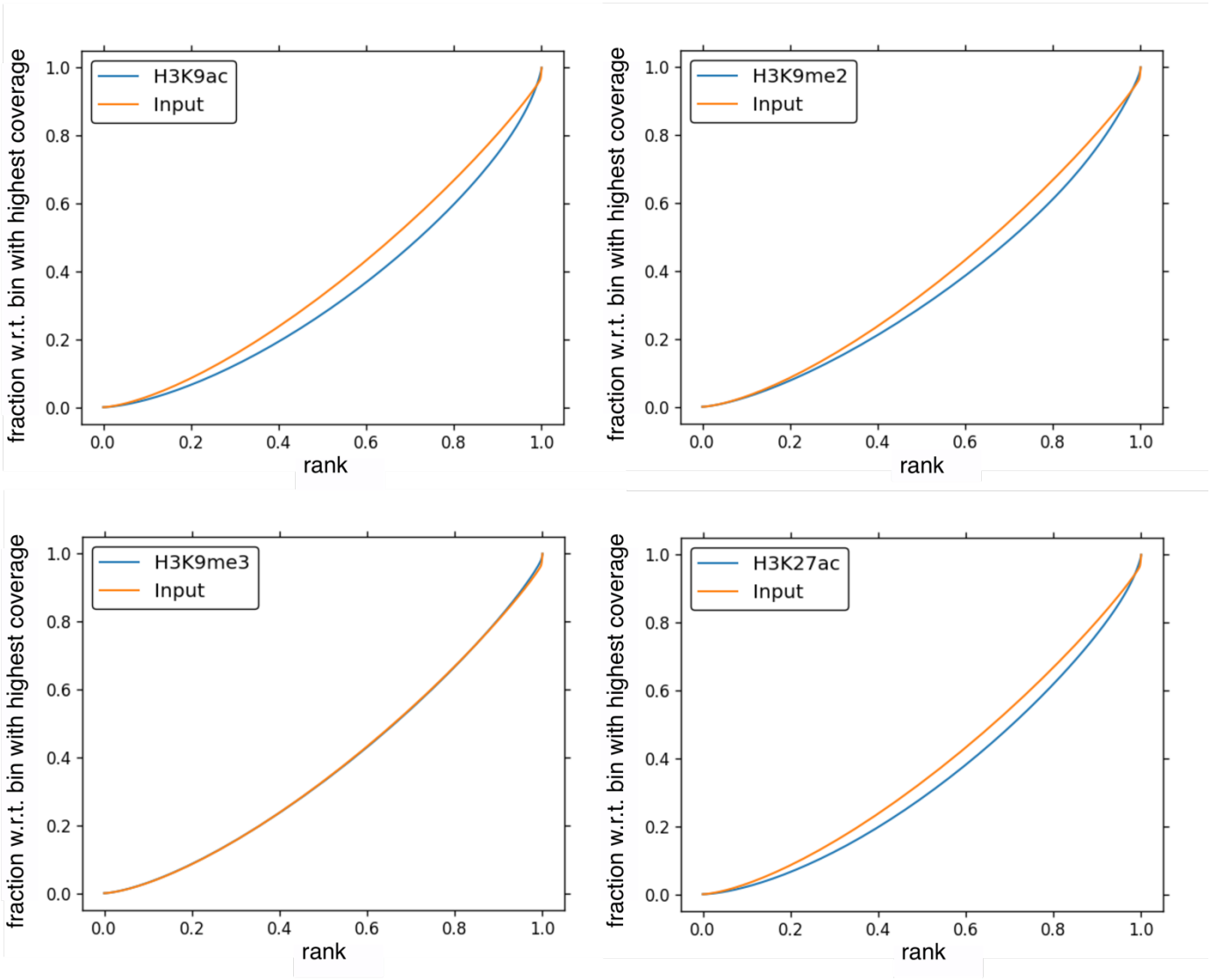

Figure S11

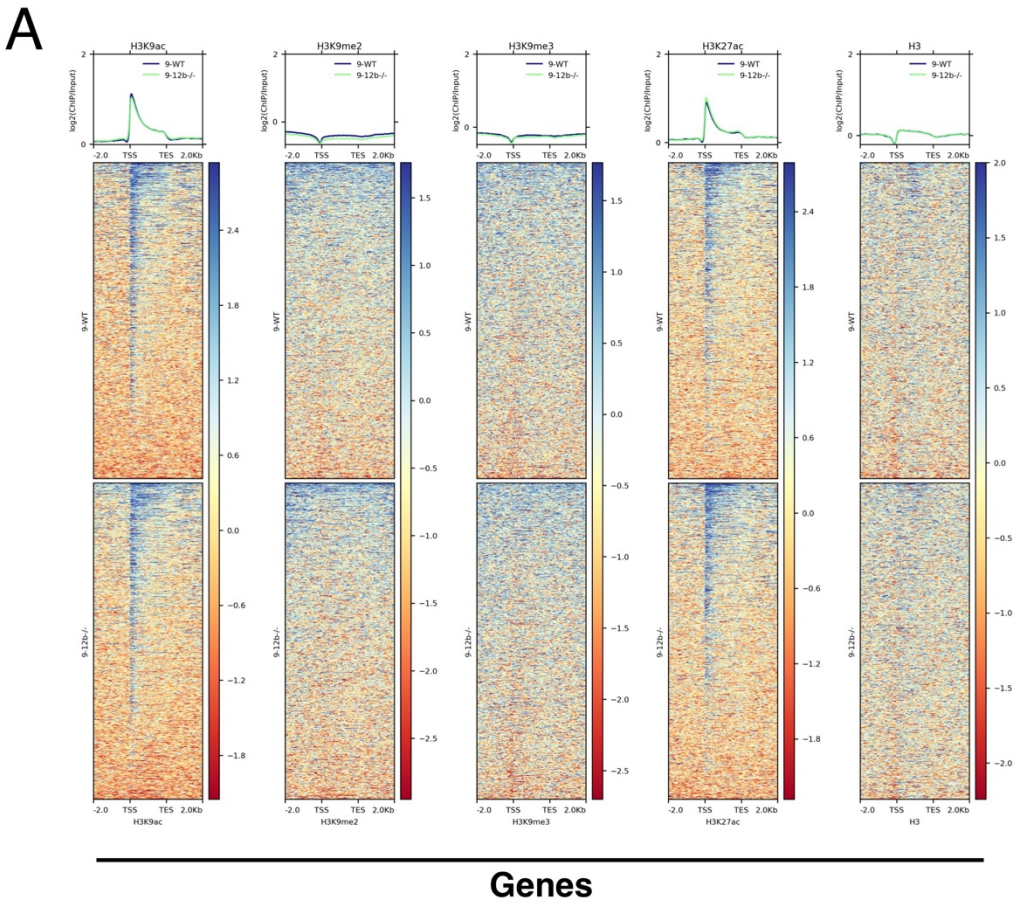

Figure S12

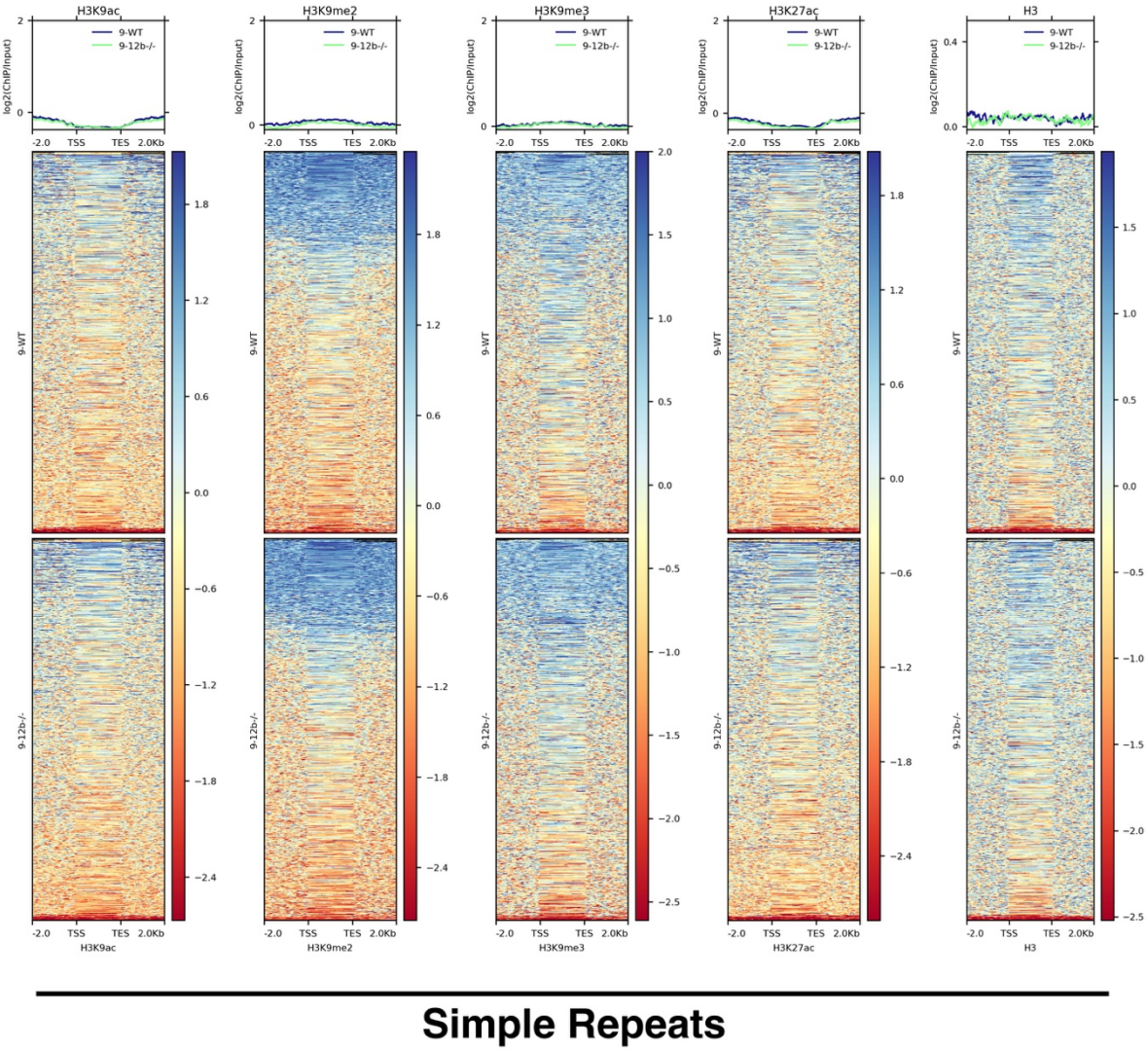

Figure S13

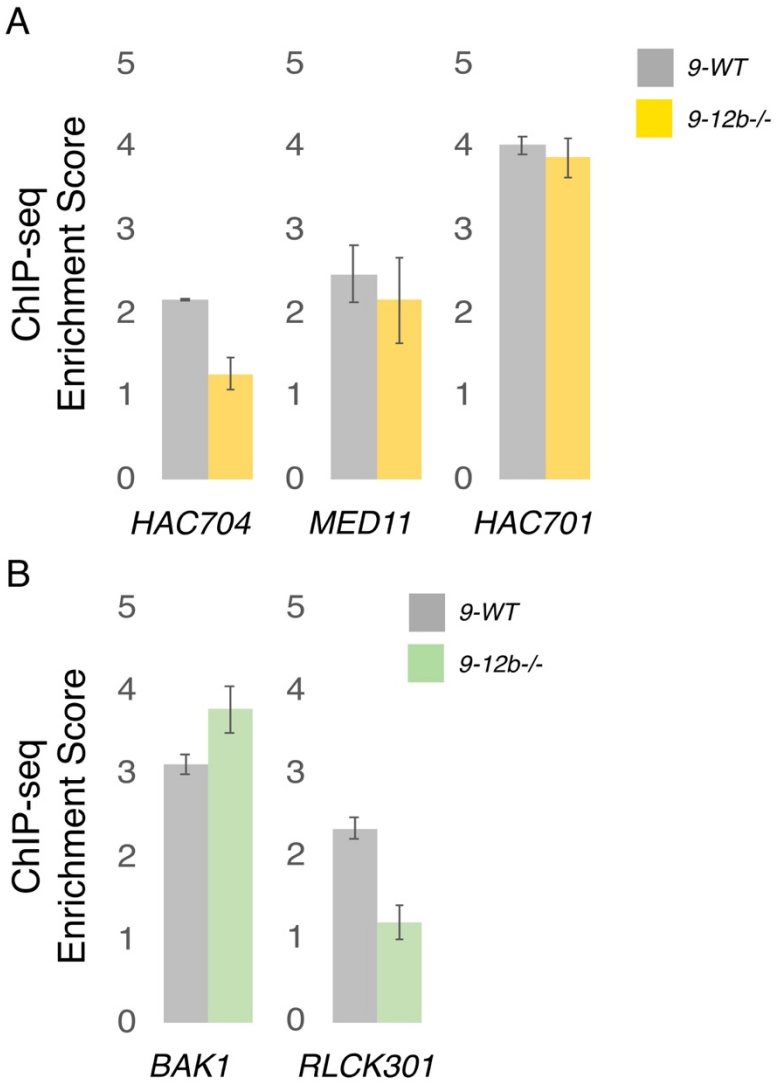

Figure S14

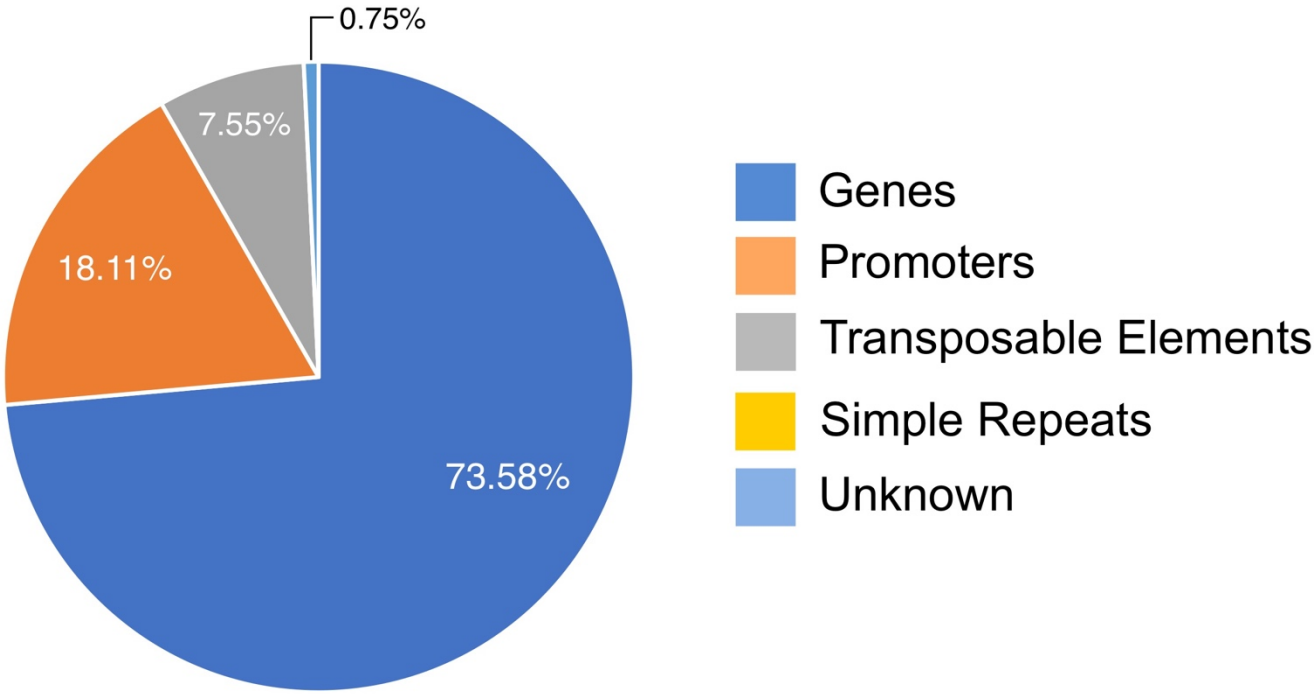

Figure S15

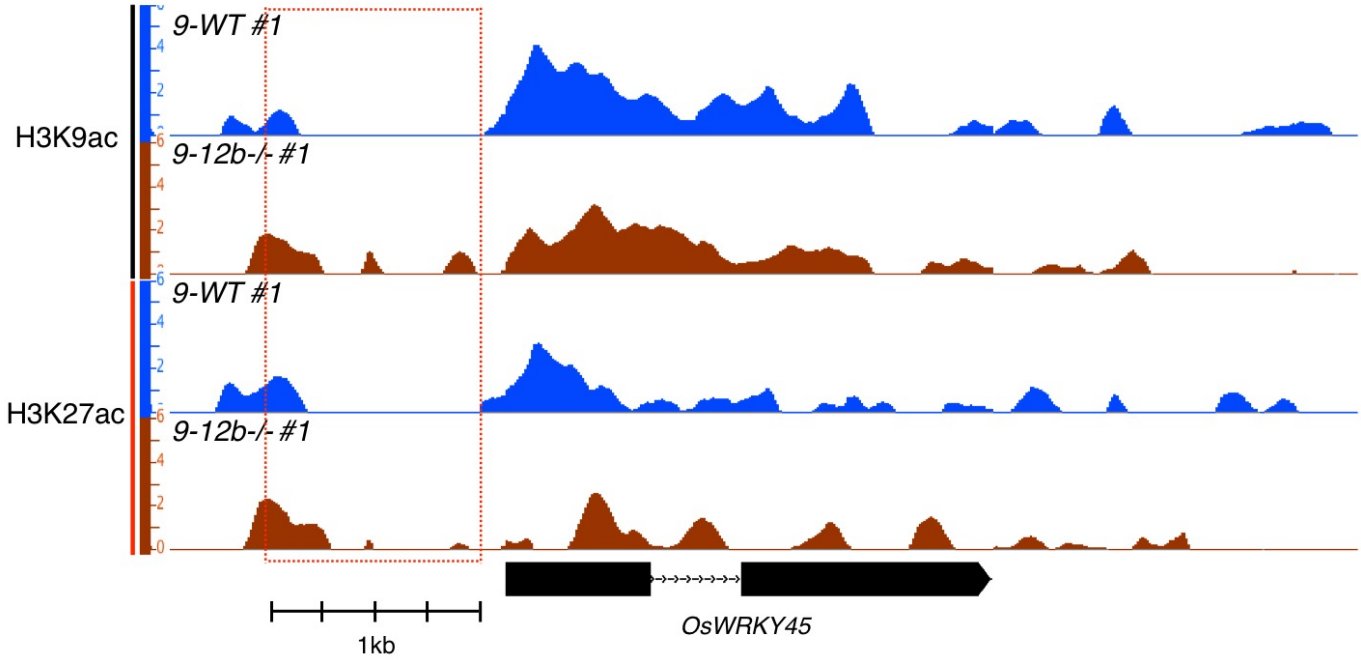

Figure S16

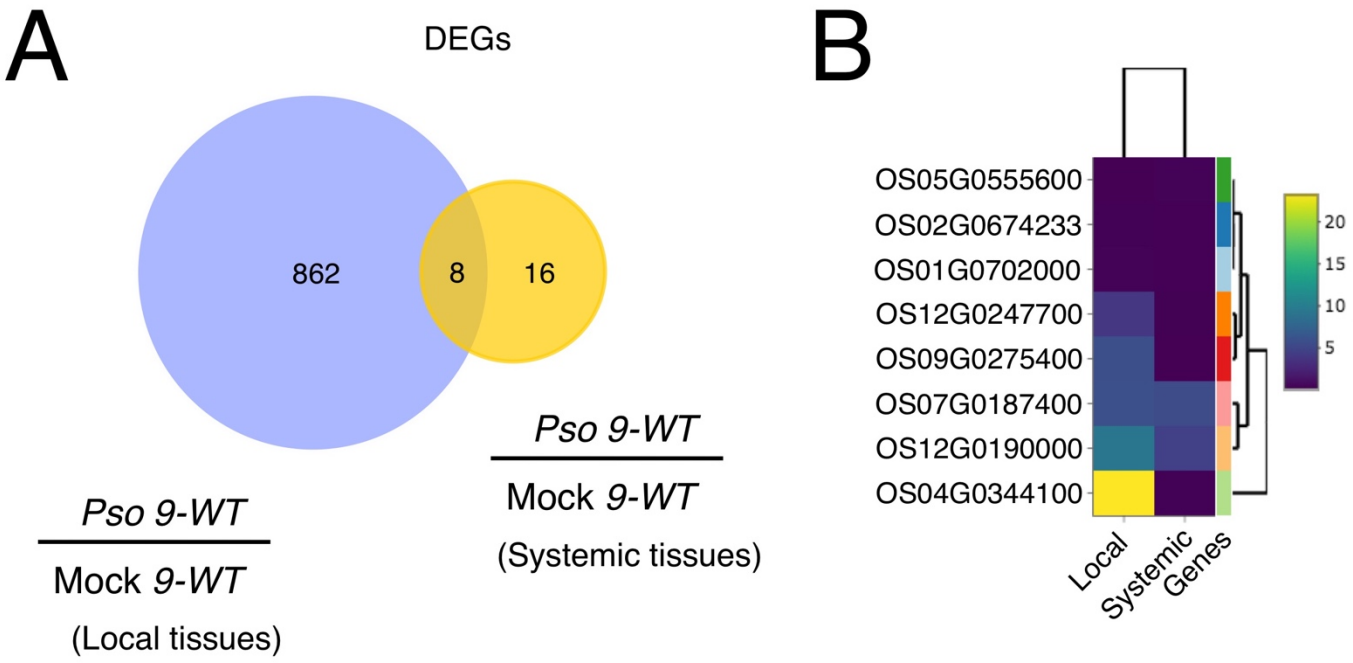

Figure S17

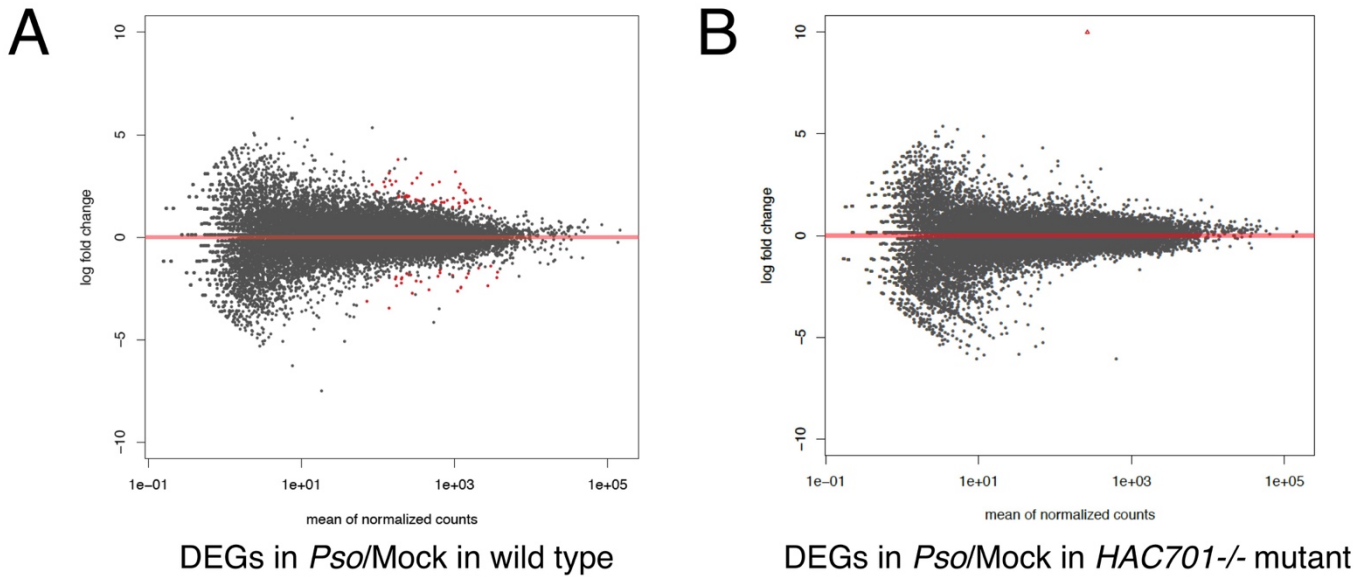

Systemic tissues

Figure S18